

**Incorporation of Ag Nanoparticles on Titania Nanotubes using
Pulse Current Deposition for Dye-Sensitized Solar Cells
Application**



By

Fatima Jamshed

(Registration No: 00000362092)

Department of Materials Engineering

School of Chemical and Materials Engineering

National University of Sciences & Technology (NUST)

Islamabad, Pakistan

(2024)

**Incorporation of Ag Nanoparticles on Titania Nanotubes using
Pulse Current Deposition for Dye-Sensitized Solar Cells
Application**



By

Fatima Jamshed

(Registration No: 00000362092)

A thesis submitted to the National University of Sciences and Technology, Islamabad,

in partial fulfillment of the requirements for the degree of

Master of Science in

Nanoscience and Engineering

Supervisor: Dr. Muhammad Irfan

School of Chemical and Materials Engineering

National University of Sciences & Technology (NUST)

Islamabad, Pakistan

(2024)

THESIS ACCEPTANCE CERTIFICATE



THESIS ACCEPTANCE CERTIFICATE

Certified that final copy of MS thesis written by Ms Fatima Jamshed (Registration No 00000362092), of School of Chemical & Materials Engineering (SCME) has been vetted by undersigned, found complete in all respects as per NUST Statues/Regulations, is free of plagiarism, errors, and mistakes and is accepted as partial fulfillment for award of MS degree. It is further certified that necessary amendments as pointed out by GEC members of the scholar have also been incorporated in the said thesis.

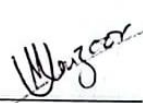
Signature: 

Name of Supervisor: Dr Muhammad Irfan

Date: 11/07/24

Signature (HOD): 

Date: 11/7/24

Signature (Dean/Principal): 

Date: 12/7/24

TH - 1

NSE-09-2021



Form TH-1

National University of Sciences & Technology (NUST)

MASTER'S THESIS WORK

Formulation of Guidance and Examination Committee (GEC)

Name: Fatima Jamshed NUST Reg No: 00000362092
Department: Department of Materials Engineering Specialization: Master of Science in Nanoscience & Engineering
Credit Hour Completed: 24.0 CGPA: 3.94

Course Work Completed

S/No:	Code:	Title:	Core/Elective:	CH:	Grade:
1.	NSE-813	Essentials of Nanoscience and Engineering	Compulsory	3.0	A
2.	MSE-854	Characterization Of Materials	Compulsory	3.0	A
3.	NSE-843	Nano Technology And Photovoltaics	Elective	3.0	A
4.	RM-898	Research Methodology	Additional	2.0	Q
5.	MSE-856	Nano Material and Processing	Compulsory	3.0	A
6.	MSE-862	Electronic And Magnetic Materials	Elective	3.0	A
7.	MSE-952	Materials For Biomedical Applications	Elective	3.0	A
8.	MSE-954A	Advanced Characterization Of Materials	Elective	3.0	A
9.	ESE-904	Advanced Energy Materials: Synthesis & Characterization	Elective	3.0	B+

Date 12-Nov-2022

Student's Signature

Thesis Committee

- Name: Muhammad Irfan (Supervisor)
Department: Department of Materials Engineering
- Name: Sofia Javed (Internal)
Department: Department of Materials Engineering
- Name: Muhammad Aftab Akram (Internal)
Department: Department of Materials Engineering
- Name: Mohsin Saleem (Internal)
Department: Department of Materials Engineering
- Name: Muhammad Irfan (External)
Department: Department of Materials Engineering

Signature

Signature

Signature

Signature

Signature

For M. Irfan

TH - 4



National University of Sciences & Technology (NUST)

FORM TH-4

MASTER'S THESIS WORK

We hereby recommend that the dissertation prepared under our supervision by

Regn No & Name: 00000362092 Fatima Jamshed

Title: Incorporation of Ag Nanoparticles on Titania Nanotubes using Pulse Current Deposition for Dye-sensitized Solar Cells Application.

Presented on: 14 Jun 2024 at: 1430 hrs in SCME (Seminar Hall)

Be accepted in partial fulfillment of the requirements for the award of Masters of Science degree in Nanoscience & Engineering.

Guidance & Examination Committee Members

Name: Dr Mohsin Saleem

Signature: Mohsin Saleem

Name: Dr Sofia Javed

Signature: Sofia Javed

Name: Dr Muhammad Aftab Akram

Signature: M. Aftab Akram

Name: Dr Tayyaba Ghani (Co-Supervisor)

Signature: Tayyaba Ghani

Supervisor's Name: Dr Muhammad Irfan

Signature: M. Irfan

Dated: 14/06/24

[Signature]

Head of Department

Date 14/6/24

[Signature]

Dean/Principal

Date 14/6/24

School of Chemical & Materials Engineering (SCME)

AUTHOR'S DECLARATION

I Fatima Jamshed hereby state that my MS thesis titled “Incorporation of Ag Nanoparticles on Titania Nanotubes using Pulse Current Deposition for Dye-Sensitized Solar Cells Application” is my own work and has not been submitted previously by me for taking any degree from National University of Sciences and Technology, Islamabad or anywhere else in the country/ world.

At any time if my statement is found to be incorrect even after I graduate, the university has the right to withdraw my MS degree.

Name of Student: Fatima Jamshed


Date: 19 February 2024

PLAGIARISM UNDERTAKING

I solemnly declare that research work presented in the thesis titled “Incorporation of Ag Nanoparticles on Titania Nanotubes using Pulse Current Deposition for Dye-Sensitized Solar Cells Application” is solely my research work with no significant contribution from any other person. Small contribution/ help wherever taken has been duly acknowledged and that complete thesis has been written by me.

I understand the zero-tolerance policy of the HEC and National University of Sciences and Technology (NUST), Islamabad towards plagiarism. Therefore, I as an author of the above titled thesis declare that no portion of my thesis has been plagiarized and any material used as reference is properly referred/cited.

I undertake that if I am found guilty of any formal plagiarism in the above titled thesis even after award of MS degree, the University reserves the rights to withdraw/revoke my MS degree and that HEC and NUST, Islamabad has the right to publish my name on the HEC/University website on which names of students are placed who submitted plagiarized thesis.

Student Signature: : 

Name: Fatima Jamshed

DEDICATION

"I dedicate this thesis to my loving parents and sisters, who loved me always unconditionally and their support inspired me for hardworking and struggle for the things that I aspire to achieve. I am really thankful to all of my friends and lab mates for their kind support and guidance."

ACKNOWLEDGEMENTS

In the beginning, I would want to convey my appreciation to Almighty ALLAH, the creator of everything, and my reverence for His Prophet Muhammad (PBUH, on whom ALLAH bestows blessings and salutations). In fact, without His blessings, this difficult and diligent task would have been impossible.

I am greatly appreciative to my supervisor **Muhammad Irfan**; under whose expertise I accomplished this research. His agility of mind and clarity of ideas put my research on track. His kindness and support beyond expression and words fall deficient to express my appreciation. I believe that without his constant and brilliant supervision I couldn't have completed my research.

I would like to offer my heartfelt thanks and appreciation to my co-supervisor **Dr. Tayyaba Ghani**, for her support and help. I am really grateful and indebted to her for sharing her experience, helpful advice, and support with me. She was very kind and cool mind towards me throughout this research. I am once again grateful to her.

I would like to thank all of the faculty members of the department for their help and support. I also want to appreciate my parents and siblings for their inspiration, help, love, and care.

I would also like to express my sincere thanks to everyone who has helped out in this initiative, whether directly or indirectly.

I pay my regards to my GEC members for their utmost support and guidance throughout this research project.

Fatima Jamshed

TABLE OF CONTENTS

ACKNOWLEDGEMENTS	IX
TABLE OF CONTENTS	X
LIST OF TABLES	XIII
LIST OF FIGURES	XIV
LIST OF SYMBOLS, ABBREVIATIONS AND ACRONYMS	XVI
ABSTRACT	XVIII
CHAPTER 1: INTRODUCTION	1
1.1 Non-conventional energy sources	1
1.1.1 Tidal Energy	2
1.1.2 Wind Energy	2
1.1.3 Bioenergy	2
1.1.4 Hydropower	3
1.1.5 Geothermal	3
1.1.6 Solar Energy	4
1.2 Solar Cells	5
1.2.1 Working mechanism	5
1.2.2 Classifications:	6
1.2.3 1 st Generation	6
1.2.4 2 nd Generation	7
1.2.5 3 rd Generation	8
1.3 Research proposal	9
1.4 Objectives	9
CHAPTER 2: LITERATURE REVIEW	10
2.1 Dye-Sensitized Solar Cells (DSSCs)	10
2.1.1 Components of DSSC	11
2.1.2 Dyes/Sensitizers	11
2.1.3 Electrolyte in DSSCs	11
2.1.4 Counter electrodes	11
2.1.5 The nanostructured metal oxide photoanode	12
2.1.6 Principle of DSSCs	12
2.1.7 Performance Factors of DSSCs	13
2.2 TiO₂ Based DSSCs	14
2.3 TiO₂ Nanotubes	16
2.4 Ag nanoparticles (NPs) deposited TiNTs	17
CHAPTER 3: MATERIALS AND METHODS	19

3.1	Material preparation	19
3.2	Materials	19
3.3	Material synthesis	19
3.3.1	Synthesis of TiNTs by anodization method	19
3.3.2	Synthesis of AgNPs/TiNTs by PCD	20
3.4	DSSC Fabrication of TiNTs and AgNPs/TiNTs composite	22
3.5	Anodization	22
3.5.1	Steps of anodization process	23
3.6	Pulse Current Deposition (PCD)	25
3.6.1	Steps of PCD	25
3.7	DSSCs Fabrication Techniques	27
3.7.1	Sealed	27
3.7.2	Microfluidic	27
3.8	Characterization Techniques	28
3.9	X-rays Diffraction (XRD)	29
3.9.1	Working principle of XRD	30
3.9.2	Components of an XRD System	30
3.9.3	XRD Techniques	31
3.9.4	Applications of X-ray Diffraction	31
3.10	Scanning Electron Microscopy (SEM)	32
3.10.1	Working principle of SEM	32
3.10.2	Components of a Scanning Electron Microscope	32
3.10.3	Types of Imaging in SEM	33
3.10.4	Applications of Scanning Electron Microscopy	33
3.11	Energy Dispersive X-ray Spectroscopy (EDX or EDS)	34
3.11.1	Working principle of EDX	34
3.11.2	Components of an EDX System	34
3.11.3	Key Features of EDX	35
3.11.4	Applications of EDX	35
3.12	Raman Spectroscopy	36
3.12.1	Principle of Raman Spectroscopy	36
3.12.2	Parts of a Raman Spectrometer	37
3.12.3	Raman Spectroscopy Modes	37
3.12.4	Applications of Raman Spectroscopy	38
3.13	Photoluminescence Spectroscopy (PL)	38
3.13.1	Principle of PL Spectroscopy	39
3.13.2	Components of a PL Setup	39
3.13.3	Types of Photoluminescence	39
3.13.4	Applications of PL Spectroscopy	40
3.14	DSSCs characterization (IV)	41
3.14.1	Solar cells characteristics parameters	41
CHAPTER 4: RESULTS AND DISCUSSION		43
4.1	Current-time curve	43
4.2	Morphological and elemental analysis	44
4.2.1	Scanning Electron Microscopy	44
4.2.2	Energy Dispersive X-ray Spectroscopy	48

4.3	Structural analysis	50
4.3.1	X-ray diffraction (XRD)	50
4.3.2	Raman Spectroscopy	53
4.4	Optical properties	56
4.4.1.	Photoluminescence spectroscopy	56
4.5	Electrical properties	59
4.5.1.	DSSCs measurements	59
CHAPTER 5: CONCLUSIONS AND FUTURE RECOMMENDATION		66
5.1	Conclusion	66
5.2	Future Recommendations	67
REFERENCES		68

LIST OF TABLES

Table 4.1: Effect of pulse current density on size of AgNPs.	46
Table 4.2: Photovoltaic characteristics of dye-sensitized solar cells using pure TiNTs and AgNPs/TiNTs.	60
Table 4.3: Photovoltaic characteristics of dye-sensitized solar cells using AgNPs/grassyTiNTs at 10, 15 and 25 mA/cm ² pulse currents.	62

LIST OF FIGURES

Figure 1.1: Projected world energy demand [1]	1
Figure 1.2: Basic Photovoltaic Cell [21]	6
Figure 1.3: Multi-Crystalline Silicon Solar Cell panel [16]	7
Figure 1.4: Thin-Film Cell [16]	7
Figure 1.5: Organic solar cell [23].....	8
Figure 2.1: Schematic illustration of a DSSC [17]	10
Figure 3.1: Schematic illustration of an electrochemical system and the production of TiNTs on Ti sheet [86].....	20
Figure 3.2: Schematic illustration of PCD set-up and AgNPs deposition on TiNTs.....	21
Figure 3.3: Schematic illustration of AgNPs/TiNTs fabrication process.	21
Figure 3.4: Schematic representations of DSSCs using (a)bare TiNTs (b)AgNPs/TiNTs [87].....	22
Figure 3.5: Schematic diagram of anodizing cell [88].....	23
Figure 3.6: Anodization process [89]	24
Figure 3.7: Set-up of PCD [90].....	25
Figure 3.8: Schematic representation of the stepwise procedure of DSSC fabrication [7]	27
Figure 3.9: Schematic representation of microfluidic DSSC [8].....	28
Figure 3.10: STOE Stadi MP XRD [95].....	29
Figure 3.11: X-ray Scattering [96].....	30
Figure 3.12: Schematic representation of XRD system [97]	31
Figure 3.13: JEOL JSM 6490A figure and schematic [98]	32
Figure 3.14: Schematic drawing of Scanning Electron Microscope [99].....	33
Figure 3.15: EDX measurement inside the SEM [100]	34
Figure 3.16: EDX Set-up [101].....	35
Figure 3.17: Schematic illustration of Raman spectrometer [103]	36
Figure 3.18: Raman Scatterings [104]	37
Figure 3.19: PL Spectrometer [105]	38
Figure 3.20: Experimental setup of PL [106]	39
Figure 3.21: Absorption and emission paths of photon [107]	40
Figure 3.22: Characteristic curve of solar cell [108]	41
Figure 4.1: Current-time plots during the first- and second-step anodization of Ti.	43
Figure 4.2: SEM images of open (a) and grassy TiNTs (b).....	44
Figure 4.3: SEM images of open TiNTs (a, b) and AgNPs/open TiNTs obtained at different pulse currents: (c, d) 10 mA/cm ² , (e) 15 mA/cm ² , and (f) 25 mA/cm ²	46
Figure 4.4: SEM images of AgNPs/grassy TiNTs obtained at different pulse currents: (a) 10 mA/cm ² , (b) 15 mA/cm ² and (c) 25 mA/cm ²	47
Figure 4.5: EDX patterns of open (a) and grassy TiNTs (b).	48
Figure 4.6: EDX patterns of (a) open TiNTs, (b) 10-AgNPs/open TiNTs, (c) 15-AgNPs/open TiNTs, (d) 25-AgNPs/open TiNTs.....	49

Figure 4.7: EDX patterns of (a) 10-AgNPs/grassy TiNTs, (b) 15-AgNPs/grassy TiNTs, (c) 25-AgNPs/grassy TiNTs.	50
Figure 4.8: XRD patterns of open and grassy TiNTs.	51
Figure 4.9: XRD patterns of open TiNTs and AgNPs/open TiNTs at 10, 15 and 25 mA/cm ² pulse currents.	52
Figure 4.10: XRD patterns of AgNPs/grassyTiNTs at 10, 15 and 25 mA/cm ² pulse currents.	53
Figure 4.11: Raman spectra of open and grassy TiNTs.	53
Figure 4.12: Raman spectra of open TiNTs and AgNPs/open TiNTs at 10, 15 and 25 mA/cm ² pulse currents.	54
Figure 4.13: Raman spectra of AgNPs/grassy TiNTs at 10, 15 and 25 mA/cm ² pulse currents.	55
Figure 4.14: PL spectra of open and grassy TiNTs.	56
Figure 4.15: PL spectra of open TiNTs and AgNPs/open TiNTs at 10, 15 and 25 mA/cm ² pulse currents.	57
Figure 4.16: PL spectra of AgNPs/grassy TiNTs at 10, 15 and 25 mA/cm ² pulse currents.	58
Figure 4.17: J–V curves of DSSCs fabricated using pure open TiNTs and AgNPs/open TiNTs at 10, 15 and 25 mA/cm ² pulse currents.	59
Figure 4.18: Schematic diagram for the charge separation and migration process of AgNPs/open TiNTs composite under visible light irradiation.	61
Figure 4.19: J–V curves of DSSCs fabricated using AgNPs/grassyTiNTs at 10, 15 and 25 mA/cm ² pulse currents.	62
Figure 4.20: Schematic diagram for the charge separation and migration process of AgNPs/grassyTiNTs composite under visible light irradiation.	63

LIST OF SYMBOLS, ABBREVIATIONS AND ACRONYMS

Silver nanoparticles	Ag NPs
Dye-sensitized solar cells	DSSCs
Nanoparticles	NPs
Titanium dioxide nanotubes	TiNTs
Pulse current deposition	PCD
Photoluminescence	PL
Fluorine doped tin oxide	FTO
Highest occupied molecular orbital	HOMO
Lowest unoccupied molecular orbital	LUMO
Photo-conversion efficiency	PCE
Fill factor	FF
Open-circuit voltage	V_{oc}
Short-circuit current	I_{sc}
Short Circuit Current Density	J_{sc}
Working electrode	WE

Counter electrode CE

Reference electrode RE

ABSTRACT

Dye-sensitized solar cells (DSSCs) have gained a lot of interest, because of their high photoconversion efficiency and less cost. In this work DSSCs were fabricated with Silver (Ag) nanoparticles (NPs) decorated titanium dioxide nanotubes (TiNTs). TiNTs with two type morphologies, open and grassy were synthesized by a two-step anodization method by utilizing of Ti sheet and then depositing Ag NPs on TiNTs by pulse current deposition (PCD) method. Pulse current deposition (PCD) manufactures homogeneous nanoparticles with adjustable size distribution by changing pulse parameters. Moreover, PCD approach has never been employed for decorating Ag nanoparticles on TiNTs by tuning pulse current as photoanode in DSSCs. This research work is the first attempt to apply PCD method by tuning pulse current for increasing plasmon effect in DSSCs. Ti was first anodized in two steps at 50 V for 2 h at 20 °C in a two-electrode cell geometry for the synthesis of TiNTs with open and grassy morphologies and then deposition of Ag NPs of different sizes on TiNTs was done using PCD at pulse currents of 10, 15 and 25 mA/cm². Scanning Electron Microscopy (SEM), Energy Dispersive X-ray Spectroscopy (EDX), X-Ray Diffraction (XRD), Raman, and Photoluminescence spectroscopy (PL) were utilized to study the morphology, elemental composition, structure, and optical characteristics of the prepared samples, respectively. The samples were then utilized as a photoanode in a back-side-illuminated dye-sensitized solar cell. The effect of Ag particle size and deposition on the TiNTs as photoanode in DSSCs was studied. The results showed that Ag NPs decorated onto TiNTs with open tube tops, at a pulse current of 15 mA/cm² exhibited the maximum photoconversion efficiency (η) of 4.46% and a short-circuit current density of 9.66 mA/cm². These results suggest that TiNTs with open tube tops decorated with optimum amount of Ag NPs as a photoanode increases the efficiency of DSSCs. This method can be utilized to create various metal-loaded nanotube array materials for energy harvesting applications.

Keywords: Dye-sensitized solar cells, Silver nanoparticles, TiO₂ nanotubes, Pulse current deposition.

CHAPTER 1: INTRODUCTION

Experts expect that the globe will require 30 TW of energy resources by 2050 to sustain economic growth as shown in figure 1.1.

For a long time, mankind has relied on several conventional sources of energy including fossil fuels, oil, biomass, agricultural stalk, and many others. For many years, the usage of these fuels has resulted in several environmental concerns such as water pollution, air pollution, and wildlife extinction. The long-term use of these traditional energy sources has resulted in global warming, acid rain, and soil eruption. Due to limited reserves of conventional sources of energy and their various concerns regarding environment, we have opted non-conventional energy sources which are sustainable and clean energy sources [1].

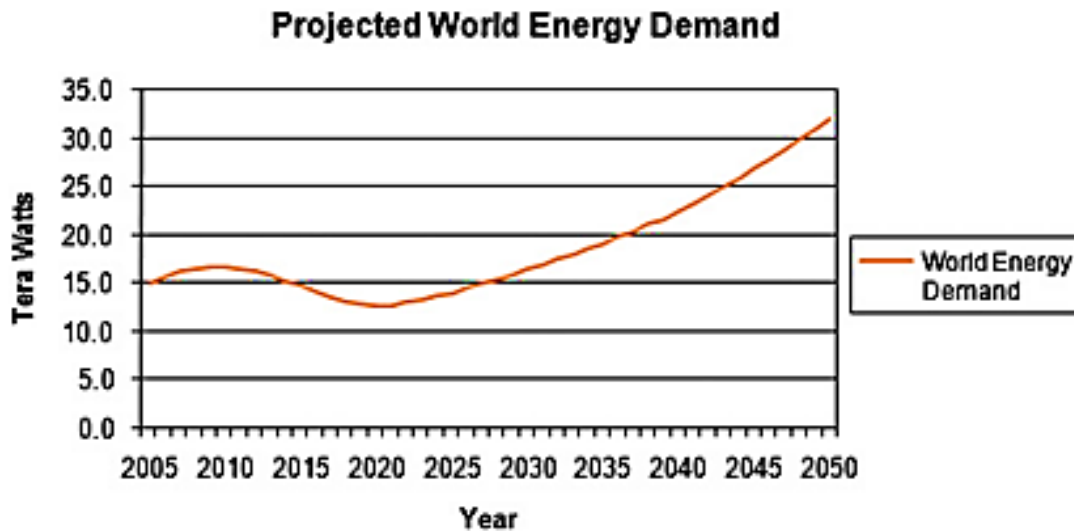


Figure 1.1: Projected world energy demand [1]

1.1 Non-conventional energy sources

Tidal, wind, biomass energy, hydropower, solar and geothermal energy are all the renewable sources of energy that can be used multiple times.

1.1.1 Tidal Energy

Tidal Energy is a new and evolving technology that is not yet economically viable and is still in the research and development phase. Tidal energy is endless source of renewable energy. It is useful because it is less prone to climate change than the other sources, which are all sensitive to unpredictable climate variations [2]. The world's potentially harvestable tidal energy supply from coastal regions is estimated to be 1 terawatt (TW). Tidal current technologies show better promise than tidal range technologies. Energy can be generated at any hour of the day or night. Furthermore, weather has little influence on tidal range [3].

1.1.2 Wind Energy

It is a type of solar energy produced when the sun heats the earth's surface unevenly. During the day, air over the land is hotter than the air over the ocean, so heated air began to expand and ascend, causing cold air rush to take the place of expanded air, generating wind [4]. Only around 2% of solar energy is converted to wind, and approximately 35% of that energy is lost within 1000 meters. Wind power has a total capacity of 1.26×10^9 MW, sufficient to meet the world's energy demand. Wind's kinetic energy is turned into its mechanical energy, which a turbine uses to generate electricity. Modern wind turbines typically have three blades and can generate power up to several megawatts at quite high wind speeds [5].

1.1.3 Bioenergy

Bioenergy can play a crucial part in attaining sustainable development [6]. Bioenergy is derived from biomass. Biomass is organic matter that is created directly or indirectly through photosynthesis using CO₂ and water from the environment in the presence of sunshine. Solar energy is stored as chemical energy, which can be transformed into electricity, heat, and transportation fuels. Biomass may comprise wood from plantation forests, leftovers from the forest, agriculture and timber industries, vegetable oil, animal fats, and organic waste from industry, animal husbandry, and human settlements [7]. There are numerous ways to turn raw biomass into usable goods. Several

conversion processes exist or are being developed to extract usable energy from biomass. In a coal-fired power plant, co-firing is the most cost-effective method. Dedicated biomass combustion units are in commercial use at both electricity and combined heat and power production (CHP) plants. Anaerobic digestion is also used in the energy generation sector and has proven to be the most suitable alternative. Further improvements will result in a cleaner, more reliable system linked to electricity, heat, and higher-quality fuel generation [8].

1.1.4 Hydropower

Hydropower is generated by moving water. It turns the kinetic and mechanical energy of water into electricity. It looks to be a type of solar energy, as the sun drives the hydrologic cycle, which facilitates rain. The hydrologic cycle brings atmospheric water to the earth's surface in the form of rain. Some of the water evaporates, but most of it seeps into the soil and becomes surface runoff. Rain and melting snow eventually reach ponds, lakes, reservoirs, and oceans and can be used to generate energy [9]. With over 150 countries producing hydroelectric electricity, hydropower is the world's greatest renewable resource and plays an essential role in many parts of the world. Norway, Bhutan, Paraguay, and numerous African countries are among the top ten countries in the world that rely nearly entirely on hydroelectric power for commercial purposes. Around 700GW of hydro capacity is estimated to be operational globally, generating 2600TWh/year (around 19% of global energy production) [10].

1.1.5 Geothermal

Geothermal energy, sometimes referred to as Earth heat, is a clean and sustainable resource. Geothermal energy is a very versatile renewable energy source, having been used for thousands of years to wash, bathe, cook, and maintain health. Direct use of hot water has a long history and is becoming more popular as new applications arise. In late 2013, twenty-four countries used geothermal energy to generate electricity, while 78 countries used it for heating. The total installed geothermal capacity in the world was 10.7GWe, and it is still expanding every day [11]. Some geothermal energy applications

rely on temperatures near the earth's surface, while others 5 require drilling kilometers underground. The three major applications of geothermal energy are as follows: [12]:

- Direct Use:** which uses hot water from adjacent reservoirs or springs.

- Power generation:** Power plants require high-temperature steam and water, ranging from 300 to 700 degrees Fahrenheit. As a result, geothermal power plants are built in areas where reservoirs are one or two miles below the surface.

- Geothermal heat pumps:** used to control building temperature by utilizing steady soil or water level near the earth's surface.

1.1.6 Solar Energy

It is very familiar form of renewable sources of energy, and it may be used in three ways: electric, thermal, and chemical. Despite the excess of solar energy, people only utilize a fraction of this immense resource. Solar energy accounts for only 0.015 percent of total global power output, and solar heat accounts for only 0.3% of global space and water heating. The most prevalent applications of solar energy include biomass production through natural processes, combustion, and gasification [13].

Many scientists feel that the sun is the only contender capable of providing a complete answer to the energy dilemma. Energy of the sun is an infinite energy source that is free to use [14]. The most significant advantage of this energy is that it has no cost and abundant when compared to the prices of different fossil fuels and oils during the last ten years [15]. Furthermore, solar energy need significantly less workforce than that required in conventional energy production technology.

Despite its immense benefits, this energy has a few drawbacks. Sun does not radiate solar energy at night. Second, solar energy does not exit continuously. To harvest electrical energy from a solar device, there must be plenty of sunshine accessible. Aside from regular oscillations in the strength of radiations, solar energy is hampered from reaching the ground during adverse weather situations. For example, the quantity of sunlight that reaches the surface of earth depends on place, timing, and weather conditions

e.g., it collapses in the winters as opposed to the summers. To address these drawbacks, sun's energy should be preserved at night, also extremely effective solar cells and panels should produce.

Even though solar energy is cost-free, there is an initial investment in the technology required to harvest this solar energy by constructing solar cells, modules and panels [16]. During operation, these small sized solar cells make no noise. On the other side, large power pumping equipments used for harvesting solar energy, causes terrible noise pollution and are hence extremely disruptive for the environment [17]. Recently, because of the diminishing supply of renewable sources of energy, expense of solar energy devices became very important in the last ten years, and it is expected that these solar energy devices will become more inexpensive in the future [18].

1.2 Solar Cells

Solar cells use photon absorption from the Sun to produce the electron-hole pairs required to generate a current. These cells are significant because they generate electricity from renewable sources, in this case the Sun.

Solar cell physics depends on the PV influence, which is the creation, trapping, recombination, and transport of charge carriers within semiconductor and between electrodes [19].

1.2.1 Working mechanism

A basic solar cell as shown in Figure 1.2, also known as a photovoltaic cell, deals with light energy of the sun and turns this energy into an electric current. The operation of these photovoltaic cells depends on three things:

- (1) Absorption of sunlight to produce electron and hole pairs
- (2) These electrons and holes pairs are separated, and
- (3) The accumulation of these electron and holes at the various electrodes to determine the difference of potential across the p-n junction. This production of potential

differential at the cell's p-n junction because of the visible radiation is used to do work [20].

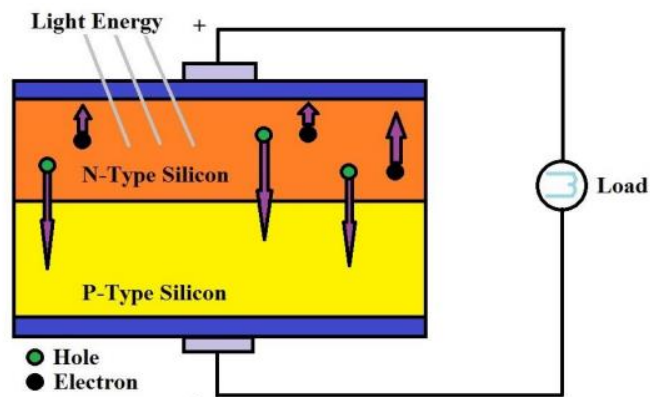


Figure 1.2: Basic Photovoltaic Cell [21]

1.2.2 Classifications:

Solar cells are classified according to the materials they are made of. Because of their distinct features, these materials are categorized into three generations:

- 1st Generation
- 2nd Generation
- 3rd Generation

1.2.3 1st Generation

Only known substance that could be utilized to construct solar cells in the beginning was Si. Si is half doped with Group-3 elements and half with Group-5 elements to form a p-n junction as shown in Figure 1.3. As a result, such solar cells are well commercialized. However, such solar cells have low efficiency in comparison to their production costs and are costly to manufacture. These type of cells can attain photo-conversion efficiency of maximum 25% [20].



Figure 1.3: Multi-Crystalline Silicon Solar Cell panel [16]

1.2.4 2nd Generation

Thin film as shown in Figure 1.4, are commonly associated with this generation. The second generation consists primarily of thin films produced through chemical and physical vapor deposition processes.

This leads to significantly cheaper production costs than their predecessors. As a result, such solar cells are less expensive yet have lower efficiency. The stated efficiencies for second generation solar cells typically range between 12 and 20%. Amorphous Silicon, Cadmium Sulfide and Cadmium Telluride are among the materials employed [20].

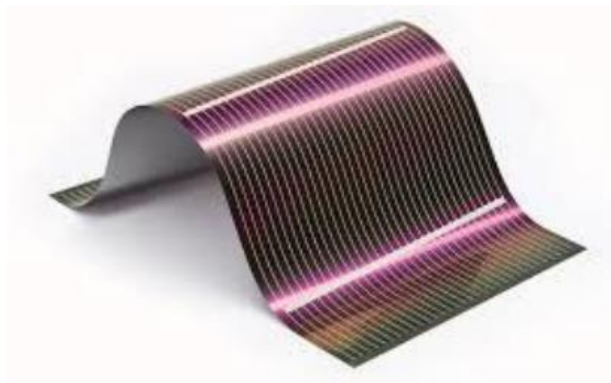


Figure 1.4: Thin-Film Cell [16]

1.2.5 3rd Generation

Solar cells of this generation can be processed in a solution. As a result, the fabrication routes for such sorts of solar cells are both chemical and physical. Because the third generation, Figure 1.5 involves nanomaterials, the fabrication routes must be carefully addressed. As a result, the cheap production costs are maintained while having substantially higher efficiency.

The efficiencies are equivalent to single crystal silicon cells, ranging from 12 to 23%. As a result, research on this generation is still ongoing, even though very little commercialization has occurred. Furthermore, this generation also includes dye sensitized solar cells (DSSC), organic solar cells, perovskite solar cells and quantum dots [22].

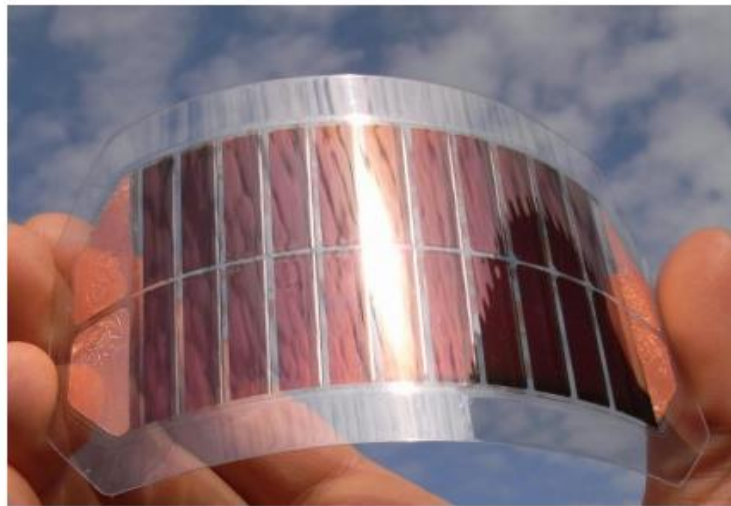


Figure 1.5: Organic solar cell [23]

To address the global need for renewable energy, new projects targeted at gathering incident photons more efficiently are needed. 1st generation (1 G) of solar cells devices are expensive to manufacture and install, but 2nd generation (2 G) of solar devices use lower cost thin films of polycrystalline semiconductors.

Moreover, their efficiencies must be improved for practical use. Recently, the emphasis is on the 3rd generation (3 G) which can deliver cost-effective, high-efficiency cells in the near future (Fig. 2) [24].

1.3 Research proposal

This study hypothesized that Silver (Ag) nanoparticles (NPs) placed on TiO₂ nanotubes (TiNTs) as photoanodes in DSSCs have higher efficiency than TiNTs due to surface plasmon resonance (SPR). It is discovered that open ended tubes with ordered morphology promotes homogeneous coverage of AgNPs, whereas defective structures promote agglomerates of AgNPs. Also, the open ended tube with ordered morphology is very effective to increase the impact of surface plasmon of Ag nanoparticles than the tubes having coverage of nanograss for the enhanced photo-conversion efficiencies of DSSCs.

1.4 Objectives

The objectives of this research are:

- To prepare the open and grassy TiNTs by anodization method.
- To deposit Ag nanoparticles on open and grassy TiNTs by pulse current deposition (PCD) method at different pulse currents.
- To characterize the prepared nanotubes by SEM, EDX, XRD, Raman and PL.
- To perform the solar cell testing of all the prepared nanotubes.

CHAPTER 2: LITERATURE REVIEW

2.1 Dye-Sensitized Solar Cells (DSSCs)

DSSCs, being extensively researched due to the secure, inexpensive, and dependable supply of energy [25]. DSSCs are promising alternatives to existing technologies due to their ease of manufacture, cost effectiveness, bifacial construction, different colour possibilities, flexibility, and maximum efficiency.

DSSCs are the solar devices that combine organic dyes (photosensitizers) and semiconductors for the production of electricity from sun-light. O Regan and Gratzel first convert the solar energy into light energy using DSSCs in 1991 [26]. Since then, research in this sector has expanded at a rapid pace, covering a wide range of vital aspects of this technology. DSSCs are widely recognized as cheap solar device because of its low-cost materials and easy construction technique. DSSCs are made up of a TiO_2 semiconductor and a dye. Furthermore, carbon based materials could be employed in place of platinum catalyst, lowering material costs even further. As a result, DSSCs are simple to manufacture because they are not sensitive and may be manufactured at room temperature. Moreover, DSSCs perform even more good in low-light circumstances, such as in twilight, dusky or cloudy weather. [27].

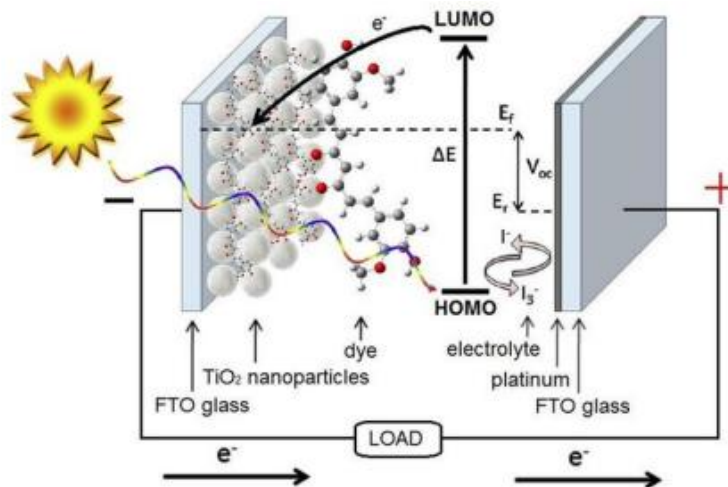


Figure 2.1: Schematic illustration of a DSSC [17]

2.1.1 *Components of DSSC*

Figure 2.1 depicts a schematic illustration of DSSCs. The system is made up of four major components:

2.1.2 *Dyes/Sensitizers*

On a metal oxide photoanode, dye molecules are chemically adsorbed. After absorbing photons of the incident light, the electron travels from HOMO to LOMO and is injected into metal oxide. Dye molecules in the DSSC produce photon-induced electrons and inject light. The quantity of dye coated on the photoanode governs the amount of dye molecules accessible for light harvesting in DSSCs, which means that the quantity of dye coated on the photoanode governs the amount of dye molecules accessible for light harvesting in DSSCs.

2.1.3 *Electrolyte in DSSCs*

Electrolyte is a DSSC component that is essential for the regeneration of oxidized dye as well as electron transport. A redox pair (I/I_3), appropriate organic solvents (to guarantee that solutes dissolve completely and are evenly dispersed), and additives (to improve durability or viscosity) are typically found in liquid electrolytes. A variety of redox combinations have been studied for faster dye regeneration and enhanced electron transportation performance. The (I/I_3) redox pair is mostly used and researched because of its low cost and ease of manufacture. As a result, it is commonly employed as standard electrolyte in DSSCs [28].

2.1.4 *Counter electrodes*

This is the DSSC construction component that completes the electrical circuit. The counter electrode surface takes electrons to decrease the oxidized redox mediator back to its non-oxidized condition. Pt-coated counter electrode is utilized for this purpose; nevertheless, the main disadvantage of Pt-coated counter electrode is its expensive cost. To cut expenses, many new counter electrodes have been constructed, including metal-

based, carbonaceous, inorganic based, and organic compound based counter electrodes [21].

2.1.5 *The nanostructured metal oxide photoanode*

In the first DSSC described in 1991 by Grätzel used TiO₂ as the photoanode material, and the photoanode layer is typically 5-20 m thick of nanomaterials [29]. This layer has a huge interior surface area that dye molecules can use to load dye to harvest sun energy. This component is essential for dye adsorption and electron transfer. Much effort has been expended on photoanode research in to increase the overall function of DSSCs. The first is to improve the light capturing capabilities of the photoanode, followed the surface alterations to improve dye loading ability and reduce recombination. Despite several attempts, the recombination issues with the TiO₂ based photoanode remain unresolved. The disadvantages of using TiO₂ mesoporous nanoparticles as photoanodes hinder DSSC development for several reasons, including: The first is poor electron movement, which leads to a high recombination rate and hence decreased efficiency; the second is an expensive method of producing nanomaterials for further dye absorption per unit volume increase; and finally, a traditional technique for the preparation of anatase TiO₂ normally necessitates high-temperature post treatments like annealing, is commonly utilized to remove impurities and increase photoanode porousness and/or crystallization of TiO₂ [30].

2.1.6 *Principle of DSSCs*

Whenever solar light reaches the cell, dye molecules on the outer layer of TiO₂ are activated, and the electrons then move towards the TiO₂ conduction band. The injected electrons move towards the anode and then do productive work at external circuit. To complete the cycle, the redox-couple electrolyte at counter electrode collects these electrons, which are then collected by dye molecules. The effectiveness of the DSSC can be measured using photo-conversion efficiency (η), Equation .1.

$$\eta = \frac{V_{oc} J_{sc} FF}{P_{in}} \times 100\% \dots\dots(1)$$

Where V_{oc} represents the open-circuit voltage (V), J_{sc} represents the short-circuit current density (mA cm^{-2}), FF represents the fill factor, and P_{in} represents incident light power. Under typical irradiation settings (100 mW/cm^{-2} , Air Mass 1.5), total photo-conversion efficiency of DSSCs is measured [31].

2.1.7 Performance Factors of DSSCs

DSSCs' performance is severely hampered by their much poorer efficiency and stability. A variety of factors effects the performance of DSSCs. The following are the three most crucial aspects:

- Inadequate light absorption
- Inadequate photovoltage output and
- Low fill factors.

The dye sensitizers utilized in DSSCs have a narrow spectrum response, which explains why light absorption is inefficient [17]. Charge recombination accounts for the low values of fill factor, whereas series resistances losses account for low photovoltage. Although several common dyes, such as

N719 dye have been observed to exhibit significant efficiency ranging from 11 to 12 percent for titania based DSSCs. However, there are several issues with these dyes, such as optimizing absorption spectra for high conversion efficiencies. These dyes have current densities that varies from 15 to 20 mA/cm^2 because of their limited absorption range, which cannot be exceeded at wavelengths beyond 800nm [17].

To reach current densities more than 25 mA/cm^2 and significantly improve the efficiency and stability of DSSCs, a concerted effort to synthesize novel dyes with a broader spectrum response is necessary. Some work has already been done to synthesize novel dyes with higher molar coefficients and a wider spectrum response, to improve the light harvesting and stability, such as ruthenium-based K-19. These new dyes are anticipated to be very beneficial in the pursuit of DSSCs efficiency greater than 12%.

Some researchers claim that by lowering the rate of recombination at the contact site of metal oxide and electrolyte, it is possible to boost efficiency by up to 50%. A few recommended techniques to increase the V_{oc} are addition of barrier layer (which can aid in interfacial recombination) and the exploration of novel electrolytes using Co-adsorbents [32].

High fill factor readings suggest that the DSSCs are operating well. Series resistance losses are the most common cause of fill factor limits. As a result, altering the contact site between the two electrodes and the wires that connects electrodes, is considered to affect the amount of series resistance. In addition to these three regulating parameters, the shape of the semiconductor layer and the fabrication conditions can affect the conversion efficiency of DSSCs. The surface area of the semiconductors should be high. The efficiency of DSSCs is also determined by particle size; higher particle sizes can improve red-light absorption in some situations, and this absorption of red light occurs because of the light scattering. Wang et.al. outlined creation of multiple layer TiO_2 nanostructures for constructing the DSSC which balances opposite impacts of light scattering and surface area, the cell's performance was increased as a result of their recommended morphology [33].

Another feature of the film's form is its thickness. The photoanode's thickness significantly affects the performance of DSSCs. Giannouli et al. did a study using Rose Bengal and Rhodamine B sensitizers. The initial goal of the research was to identify that how ZnO film thickness affects the efficiency of DSSCs. The findings revealed that there is an ideal thickness for best efficiency. Beyond this optimum thickness, either too little or too much thickness can lower conversion efficiency [34].

2.2 TiO_2 Based DSSCs

Wide bandgap semiconductors are commonly employed as photoanode materials in DSSCs because they are more stable under light. ZnO, TiO_2 , SnO_2 , Nb_2O_5 , and Fe_2O_3 are some of the widely investigated wide bandgap photoanode materials. Despite having better movement of electrons and similar band location like TiO_2 , ZnO is not the suitable material for commercial applications due to its instability in acidic dyes. Although SnO_2

has higher values of mobility but because of its quick recombination and low V_{oc} , treatments of surfaces are necessary for SnO_2 to be utilized in DSSCs. Nb_2O_5 has lower electron mobility, lower surface area and chemical instability hence it is an inappropriate material to be used as photoanode in DSSC. Fe_2O_3 has higher recombination rate, lower photocurrent density and narrower absorption spectrum which also makes it unsuitable to be used as photoanode in DSSCs.

TiO_2 is mostly used among the various materials due to its superior features. TiO_2 's C.B (Conduction band) exists lower to the LUMO (lowest unoccupied molecular orbital) state of majority of regularly utilized dyes, allowing the quicker electron transport. It has less toxicity and greater chemical stability. Also, it possesses a large refractive index that is necessary for light diffusion into the complete mesoporous layer. The large dielectric constant of TiO_2 helps in reducing quick recombination of electrons and holes pairs at the TiO_2 /dye interface site by electrostatic shielding.

Common TiO_2 's phases, such as anatase, rutile, and brookite have been studied as photoanodes in DSSCs. Anatase TiO_2 is mostly used because of its indirect bandgap that does not allow direct transfer of electrons from C.B to V.B. This TiO_2 phase has longer lifetime for photogenerated carriers than rutile and brookite. Moreover, in anatase the recombination of charge carriers is significantly lower because of its smaller photocarrier effective mass which aids in rapid migration of charge carriers.

Venkatraman Madurai et.al. prepared TiO_2 nanoparticles (NPs) utilizing the microwave and solvothermal approach for DSSCs and attained a maximum efficiency of 7.44% [35]. R.S. Dubeya et.al. prepared TiO_2 NPs by solvothermal and sol-gel method for DSSCs and achieved efficiency of 2.17% [36]. Huei-Siou Chen et.al. prepared anatase TiO_2 NPs for DSSC and achieved maximum photo-conversion efficiency of 6.61% [37].

However, the grain boundaries of TiO_2 NPs may cause electron recombination, resulting in a decrease in photocurrent and absorption of light in the near-infrared region [38].

2.3 TiO₂ Nanotubes

TiO₂ nanotubes (TiNTs) have been proposed as a beneficial photoelectrode option for DSSCs as an alternative to TiO₂ NPs. TiNTs exhibit improved light scattering inside the tubes which results in more absorption of light, rapid electron transport, less charge carrier recombination, and easy geometry when compared to NPs. Furthermore, the tubes give a relatively high contact surface area to deposit the metal oxide NPs and adsorb dye molecules [38].

Many researchers are trying to create such extraordinary nanostructured materials for utilizing them in different fields including biosensors, photocatalysts, photovoltaic, self-cleaning, water splitting, photodegradation, and adsorbents [39]. These one directional and low-dimensional titanium oxide materials have also been investigated for improved efficiencies of cheap solar cells, namely DSSCs [40].

Uchida et.al. reported a DSSC with TiNTs as the photoanode with 100 nm long TiNT having diameter of 8 to 10 nm and overall cell's active area of 25 mm². These TiNTs were generated using hydrothermal technique which demonstrated efficiency of 2.9% [41]. Later, anodic TiNTs with 500 nm and 2.5 μm tube lengths were synthesized and have PCEs of 1.6% and 3.3%, respectively [42]. Senadeera et.al. employed TiNTs as photoanodes in DSSCs and achieved a maximum photo-conversion efficiency of 8.31%. [43]. Naeimeh et.al. attained a PCE of 8% using a free-standing one-dimensional TiNTs as a photoelectrode in DSSC. [44]. Chao-Nan Chen et al. used liquid phase deposition and anodization to create TiNTs with a maximum conversion efficiency of 2.85%. [45].

Structure and crystalline nature of TiNTs are two essential criteria in its application. To enhance these criterias, these tubes have been prepared using different approaches like sol-gel [46], seed growth method [47], photoelectrochemical etching [48], hydrothermal [49], electrochemical lithography [50], template-assisted fabrication [51], atomic layer deposition [52], anodization [53], etc.

Among the above nanotube manufacturing processes, electrochemical anodization is the simplest and cheap method because it demands no special experimental system and gives good control on the morphology of tubes and pore size [54].

But the large band gap of TiO_2 in TiNTs results in poor absorption of light in the visible light spectrum, limiting its usability for different fields such as water splitting, pollutant degradation and solar cells. The fast recombination rate of charge carriers is another barrier to its use for these purposes [55].

2.4 Ag nanoparticles (NPs) deposited TiNTs

Significant attempts have made for band gap reduction and decrease the rate of recombination of charge carriers in TiO_2 for the modification of TiNTs. Ion doping of metal or nonmetal [56], sensitization of dye [42], coupling of narrow band gap semiconductor [57], and modification of noble-metal nanoparticles (NPs) [58] have all been part of these efforts [55]. Among these attempts, the alteration of TiO_2 with nanoparticles of noble metals like Ag or Au have gained attention. They are anticipated to capable of extending TiO_2 's visible light absorption and lowering the recombination rates of charge carriers because of influence of surface plasmonic resonance (SPR) caused by electron oscillations at surface. Among noble metals Ag is the most promising options for different applications, because it is cheap and can be easily prepared than other ones [59]. Untill now, plasmonic effect of Ag is mostly used in the field of photocatalysts [60, 61], biosensors [62, 63], water-splitting [64, 65] and for enhanced vascular biocompatibility [66, 67]. Ag modified TiO_2 composite have also been employed as photoanode in DSSCs [68-78]

Kawamura et al fabricated TiNTs by hydrothermal method and adsorbed Ag NPs on TiNTs by the photodeposition and achieved efficiency of 7.20%, that is greater as compare to bare TiNTs (2.83%) [79]. Won-Yeop Rho et al. fabricated TiNTs by anodization method and deposited Ag nanoparticles on them by photodeposition synthesis method. They obtained photoconversion efficiency of 6.14% which is greater than pure TiNTs (4.64%) [80]. Nyein Nyein et.al. synthesized Ag NP covered titania nanotubes and achieved efficiency 3.7% which was greater than the 3% recorded for bare nanotubes [59].

Several attempts have been used to decorate Ag NPs on the TiO₂ like photo-deposition [79, 80], calcination reduction [81, 82], and electrochemical deposition [83, 84]. But, no one is capable of preventing agglomeration of Ag nanoparticles and maintaining homogenous morphology [85]. Pulse current deposition (PCD) is a practical approach for controlling the density and element's size and achieving uniform coverage on a conductive substrate. PCD is superior than direct current plating in terms of obtaining highly-fine grained structures, more homogenous surfaces, and enhanced characteristics such as strength and hardness [85]. By changing the current-on time (t_{on}) and current-off time (t_{off}), pulse cycles, and current density via pulse control can result in highly-fine structures and a uniform surfaces. As a result, PCD can produce Ag that is equally spread having size in nano range. On the other side, direct current (DC) electro-deposition produces non-homogeneous Ag with a rough surface, making it unsuitable for manufacturing Ag nanoparticles. Furthermore, the pulse current deposition approach may easily increase the plasmon effect.

Xinning Luan et al, synthesized Ag NPs deposited on TiNTs using pulse current deposition by tuning pulse deposition time and used this composite in DSSCs and obtained efficiency of 3.82% greater than DSSCs with a photoanode made out of bare TiNTs (2.61%) [85]. However, this method has never been used for depositing Ag nanoparticles on TiNTs using pulse current deposition by tuning pulse current as photoanode in DSSC. This research work is the first attempt to use pulse current deposition method by tuning pulse current for increasing the plasmon effect in DSSCs. In this work, we investigated the pulse current deposition process further to disperse Ag NPs on TiNTs. We synthesized TiNTs with two types of morphology open and grassy by anodization of Ti sheet and then deposit Ag NPs of different sizes on TiNTs by PCD at pulse currents of 10, 15 and 25 mA/cm². The impact of Ag particle size and deposition on the TiNTs as photoanode in DSSCs was investigated. The experimental results showed that AgNPs/TiNTs composite with open tube top at 15 mA/cm² pulse current have highest photoelectric conversion efficiency of 4.46% in DSSCs.

CHAPTER 3: MATERIALS AND METHODS

3.1 Material preparation

The synthesis technique was selected depending on the cost effectiveness, ease of making, availability of in-house resources, and the reproducibility feature. Hence anodization technique was used to synthesize TiO₂ nanotubes (TiNTs) and for the further modification of nanotubes, Ag nanoparticles (NPs) were coated on them using pulse current deposition (PCD) approach.

3.2 Materials

Ti metal sheets of 25 μm thickness and purity of 99.6% were purchased by shop.solaronix.com. Solvents including acetone, ethanol, and ethylene glycol were acquired from Sigma Aldrich. NH₄F, AgNO₃ and NaNO₃ were purchased from Uni-Chem chemical reagents and Alfa Aesar respectively. DI-water was utilized in all studies.

3.3 Material synthesis

3.3.1 *Synthesis of TiNTs by anodization method*

TiNTs were prepared using a two-step anodization method. Schematic illustration of an electrochemical system and the production of TiNTs on Ti sheet is shown in Figure 3.1. Each Ti metal sheet was first cleaned with emery paper and then sonicated in three solvents: DI-water, ethanol, and acetone, respectively for the period of 15 min each. The anodization electrolyte was composed of 0.5 wt% NH₄F, 3 wt% DI-water, and ethylene-glycol. First-step anodization of Ti sheet was done by two electrodes (Ti sheet and stainless-steel sheet) cell geometry that dip in the electrolyte at a potential of 50 V for 2 h at 20 °C. The grass layer of titania oxide which was formed during the first step of anodization was cleaned up through sonication in DI-water for 15 to 20 min, yielding a polished and patterned Ti surface. The pretreated sample was then anodized in the second step for two hours under the same conditions identical to the first step. Samples were

carefully cleaned with DI water after the second step of anodization and sonicated for a few seconds in ethanol to obtain the open-ended ordered morphology of nanotubes [86].

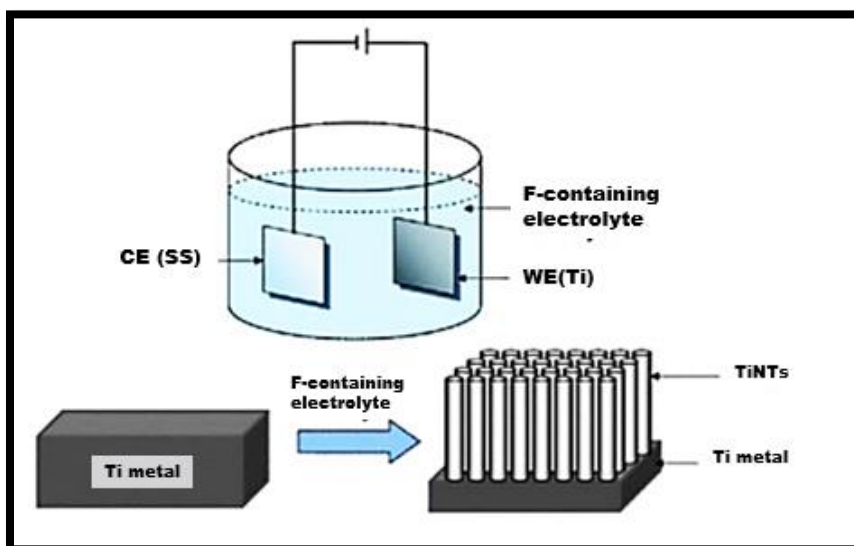


Figure 3.1: Schematic illustration of an electrochemical system and the production of TiNTs on Ti sheet [86].

3.3.2 Synthesis of AgNPs/TiNTs by PCD

In a typical procedure, silver nanoparticles (AgNPs) were coated onto the open channel titania nanotubes by utilizing a two-electrode technique with an anodized TiNTs as cathode and a rod of graphite as anode by Pulse Current Deposition (PCD) method. The electrolyte used for PCD was a 1:1 combination of 0.01 molar AgNO_3 and 0.1 molar NaNO_3 solutions by volume. Schematic diagram of PCD set-up and AgNPs deposition on TiNTs is shown in Figure 3.2. AgNPs were deposited onto TiNTs for 100 cycles at pulse currents of 10, 15, and 25 mA/cm^2 with current on-time/off-time of 1s/3s, respectively. All PCD tests were performed at room temperature using an AMEL potentiostat (2051 model) and a programmed function generator (568 type, AMEL). The AgNPs/TiNTs composites were then placed in oven for 30 min at 100 °C before being vacuum annealed at 450 °C for 2 h. Schematic illustration of AgNPs/TiNTs fabrication process is represented in Figure 3.3.

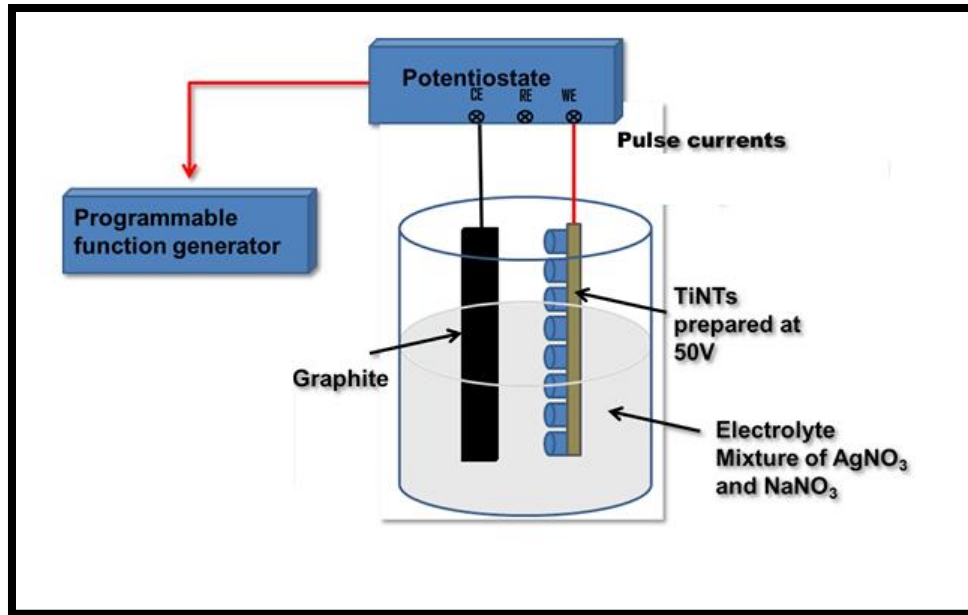


Figure 3.2: Schematic illustration of PCD set-up and AgNPs deposition on TiNTs.

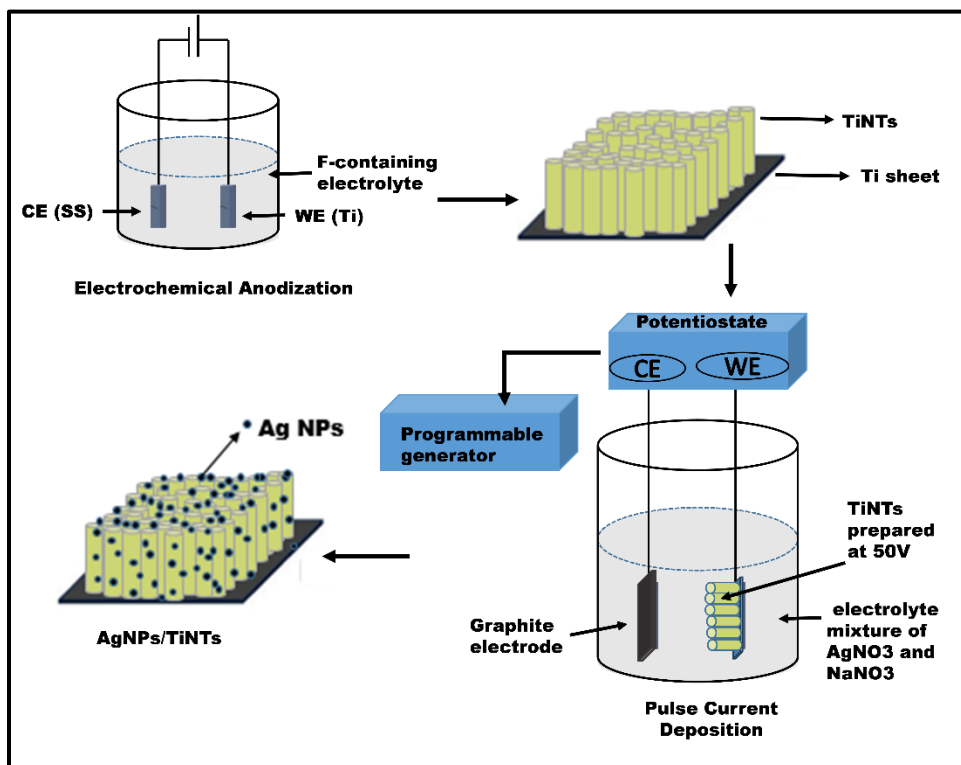


Figure 3.3: Schematic illustration of AgNPs/TiNTs fabrication process.

3.4 DSSC Fabrication of TiNTs and AgNPs/TiNTs composite

In this study, the sealing technique was used to fabricate DSSC. Schematic diagrams of DSSCs using bare TiNTs and AgNPs/TiNTs are shown in Figure 3.4 (a, b). To evaluate the photovoltaic performance, the TiNTs and AgNPs/TiNTs samples were dipped in 0.3 mM solution of N3-dye in ethanol/isopropanol (1:1) ratio for 1 day. Dye sensitized TiNTs and AgNPs/TiNTs photoanodes were sandwich by using a molten state sealant having thickness of 25 μm (Solaronix, Meltonix) with Pt coated FTO glass as counter electrode. The iodide/triiodide electrolyte (Iodolyte AN50, Solaronix) was introduced between the sandwich electrodes via vacuum back filling through a hole in the Pt electrode [87]. Cell's active area was 0.2 cm^2 , the DSSCs were then shined in back illumination mode because the Ti metal was used as substrate beneath the TiO_2 oxide.

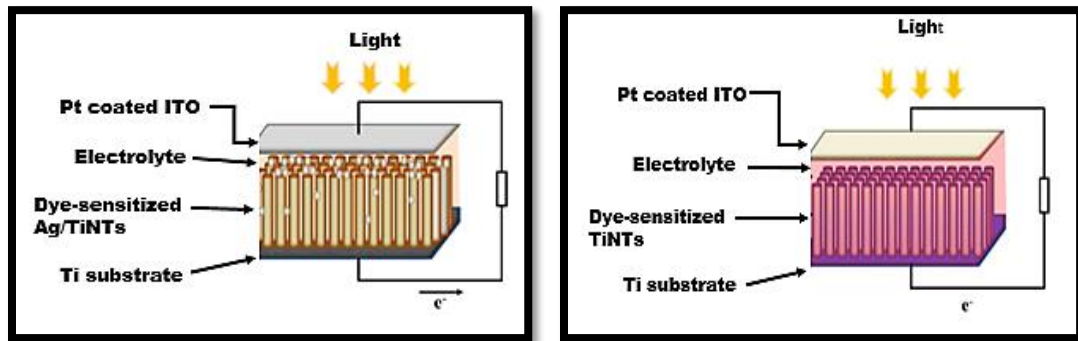


Figure 3.4: Schematic representations of DSSCs using (a) bare TiNTs (b) AgNPs/TiNTs [87].

3.5 Anodization

Anodization is an electrochemical technique that thickens the layer of natural oxide on the metal component, schematic illustration showing anodizing cell is represented in Figure 3.5.

It is frequently used to improve corrosion resistance, surface hardness, and paint or other coating adhesion. The method is commonly used on aluminium, although it can also be used to other metals such as titanium [88].

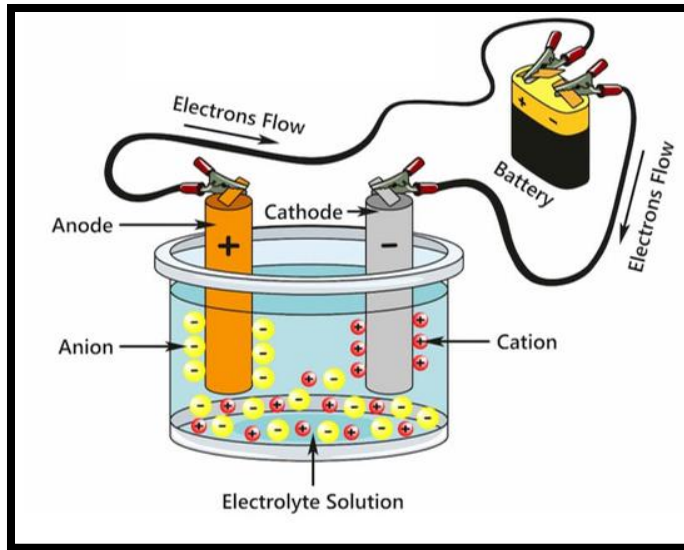


Figure 3.5: Schematic diagram of anodizing cell [88]

3.5.1 Steps of anodization process

Steps of anodization process as shown in Figure 3.6 and are given below

1. Cleaning:

To eliminate any dirt, grease, or other pollutants, the metal surface is thoroughly cleaned. This is usually accomplished through procedures like alkaline cleaning or acid etching.

2. Etching:

Etching is a vital procedure conducted before anodization of metal to increase final treatment quality. Etching removes any surface impurities or oxides from the component, resulting in a clean and uniform surface that can be anodized more easily.

3. Desmutting:

Desmutting is the process of removing excess alloyed metals from the surface of metals after they have been etched. It can be performed in any mineral inorganic acid, such as hydrochloric, sulfuric, nitric, and so on.

4. Anodization:

Immersion in Electrolyte: For anodization, the prepared metal is immersed in an electrolyte bath containing Fluoride ions.

Application of current: A direct current (DC) is passed through the metal, which serves as the anode, with a cathode (typically constructed of lead or aluminium) completing the circuit.

Oxide layer Formation: Ions of oxygen are released at the anode and interacts with the metal surface to generate a thick, porous oxide layer. By altering the voltage and time of the anodization method, the amount of thickness of this porous oxide layer can be adjusted.

5. Coloring (Optional):

To create a desired colour, the porous anodic oxide layer can be coloured. This is frequently accomplished by dipping the anodized component in a solution having organic or inorganic colours.

6. Sealing:

To close the holes in the oxide layer and improve corrosion resistance, the anodized part is frequently sealed. This can be accomplished using hot water sealing or other sealing methods [89].

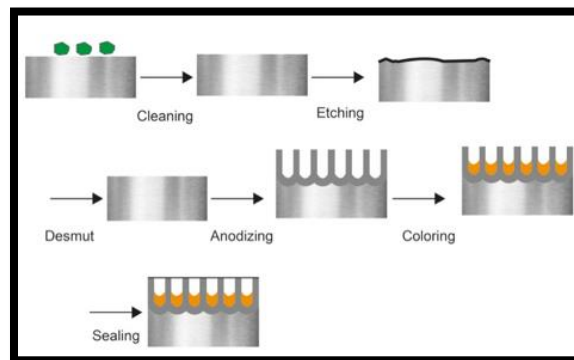


Figure 3.6: Anodization process [89]

3.6 Pulse Current Deposition (PCD)

Pulse current deposition is a type of electrodeposition that employs alternating current with periodic interruptions or pulses as shown in Figure 3.7. This approach is used to improve certain attributes of the deposited metal layer, such as adhesion, thickness, or microstructure control. Compare to typical direct current (DC) approaches, pulse current offers greater control over the deposition process [90].

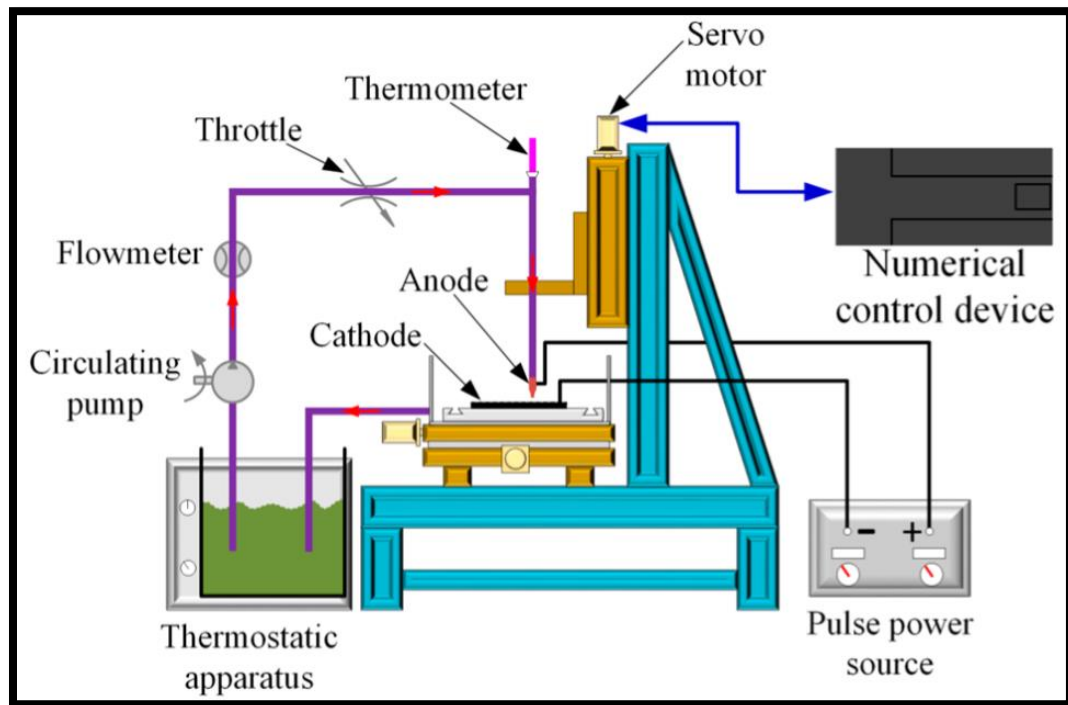


Figure 3.7: Set-up of PCD [90]

3.6.1 Steps of PCD

1. Preparation:

Substrate preparation: The substrate (material to be coated) is properly cleansed to remove any impurities, ensuring that the deposited layer adheres well.

Electrolyte selection: Based on the metal to be deposited and the desired coating qualities, an appropriate electrolyte solution is selected.

2. Set up:

Electrochemical cell: The substrate and counter electrode are dip in electrolyte solution. The positive terminal (anode) is connected to the substrate, while the negative terminal (cathode) is connected to the counter electrode. [91].

Pulse generator: To control the pulsating current applied to the system, a pulse generator is used. The pulse frequency, duty cycle, and peak current of the generator can all be adjusted.

3. Pulse current deposition:

Pulse on-time: In the electrolyte the ions of metals are reduced and deposited onto the substrate during the "on" time of each pulse.

Pulse off-time: The "off" time of each pulse allows for relaxation of the deposited layer, ion diffusion, and other electrochemical activities.

4. Parameters optimization:

Pulse frequency: The frequency at which pulses are applied, measured in hertz (Hz).

Duty cycle: The pulse-on time to total pulse period ratio, presented as a percentage.

Peak current: The maximum current during pulse-on time.

5. Monitoring and Control:

Process Monitoring: During the procedure, parameters like deposition rate, thickness, and surface morphology are measured.

Feedback Control: Some systems may have feedback control mechanisms that allow pulse settings to be adjusted in real time based on monitoring results.

6. Post Treatment (Optional):

Annealing or Heat Treatment: Post-treatment processes such as annealing may be used depending on the application to improve the properties of the deposited layer [92].

3.7 DSSCs Fabrication Techniques

Two DSSCs fabrication techniques are commonly used

- Sealed
- Microfluidic Structure

3.7.1 Sealed

A sandwich-like cell as shown in Figure 3.8, is created in this technique by using a metal oxide working electrode and a hole-drilled counter electrode in a manner that both remain face-to-face. As a sealant, a 30 μm thick Surlyn thermoplastic is employed and modified such that the interior dimensions match with the active area of cell's working electrode. The final sealed DSSC is created by combining heat with holes in the counter electrode for electrolyte entry [93].

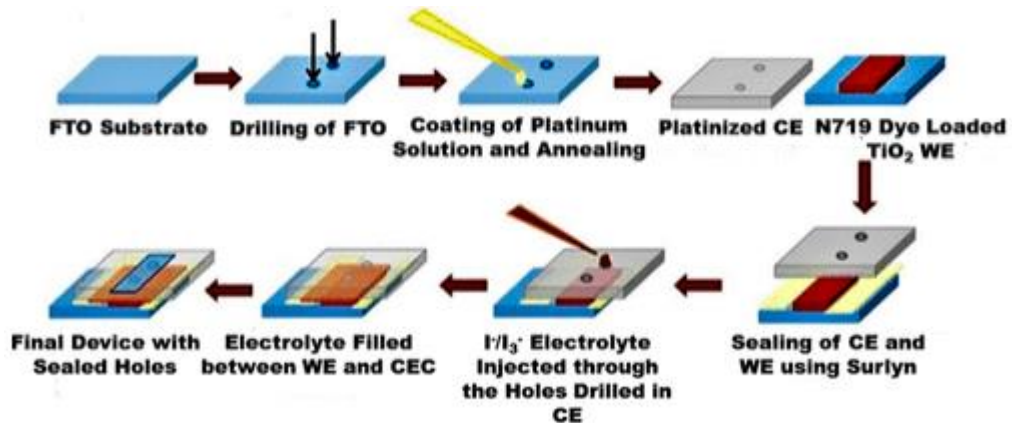


Figure 3.8: Schematic representation of the stepwise procedure of DSSC fabrication [7]

3.7.2 Microfluidic

The microfluidic structure is a reusable clamping device used in the manufacture of DSSCs that ensures the sealing to prevent electrolyte leakage as shown in Figure 3.9.

Two polymethylmethacrylate (PMMA) exterior clamping structures with holes for screw tightening are employed in this construction procedure to hold all the components in place. A membrane made of PDMS pre-polymer and curing agent is inserted between a photoanode and a counter electrode. Photoanode and counter electrodes are mounted on PMMA structures in such a way that electrolyte can flow between the electrodes via housing openings. Copper foils are used to connect the photoanode and counter electrode [94].

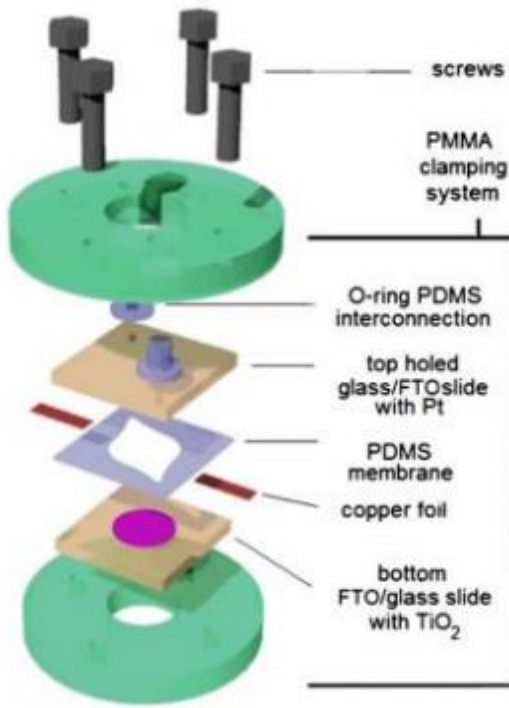


Figure 3.9: Schematic representation of microfluidic DSSC [8]

3.8 Characterization Techniques

The results attained by using various characterization techniques:

- X-rays Diffraction (XRD)
- Scanning Electron Microscopy (SEM)
- Raman Spectroscopy

- Photoluminescence (PL) Spectroscopy
- Diffuse Reflectance Spectroscopy (DRS)
- DSSCs Characterization

3.9 X-rays Diffraction (XRD)

It is a strong method that analyzes the diffraction pattern formed when X-rays incident on a sample to discover the crystallographic structure of a material. This approach is mostly used in materials science, chemistry, geology, and other scientific disciplines [95]. X-ray diffractometer is shown Figure 3.10.



Figure 3.10: STOE Stadi MP XRD [95]

3.9.1 Working principle of XRD

Diffraction happens when X-rays incident on a crystalline material and resulting scattered waves interfere constructively as shown in Figure 3.11. The resulting diffraction pattern gives information about the crystal structure, including lattice parameters, crystal orientation, and phase identification. Schematic illustration of XRD system is represented in Figure 3.12.

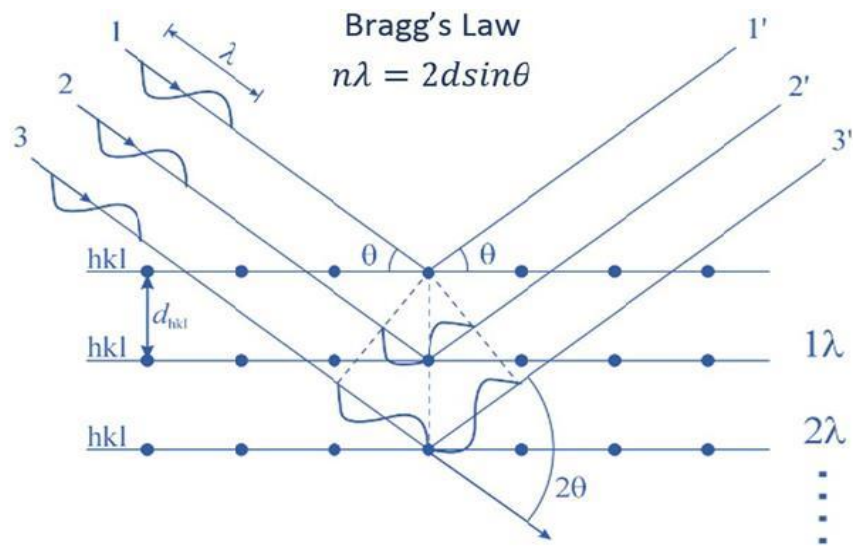


Figure 3.11: X-ray Scattering [96]

3.9.2 Components of an XRD System

X-ray Source: A revolving anode or sealed X-ray tube that emits monochromatic X-rays.

Sample Holder: Maintains a specific orientation for a powdered or crystalline sample.

Detector: It measures the strength of diffracted rays from multiple angles.

Analyzer: Monochromator or crystal that selects a specific X-ray wavelength. [96].

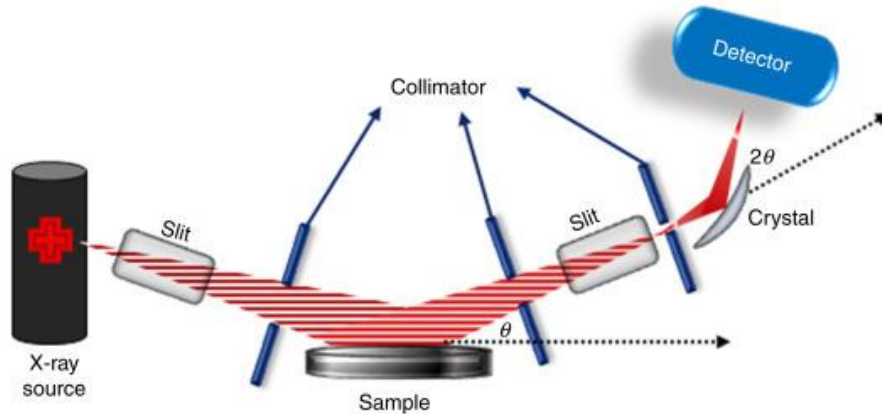


Figure 3.12: Schematic representation of XRD system [97]

3.9.3 XRD Techniques

Powder XRD (XRPD): A method used to identify different crystalline phases and crystal structure in powdered samples.

Single Crystal X-ray Diffraction: For single crystals, this technique provides extensive information about the atom arrangement in the crystal lattice.

Thin Film X-ray Diffraction: Used on thin films to determine thickness and crystallographic orientation.

3.9.4 Applications of X-ray Diffraction

Materials science: Study of crystal structures, phase identification, and defect analysis in materials.

Geology: Scientific study of minerals and geological formations.

Pharmaceuticals: Crystal structure characterization in medication development.

Biology: Analysis of protein and DNA crystal structures.

Quality control: Identifying and quantifying phases in industrial processes [97].

3.10 Scanning Electron Microscopy (SEM)

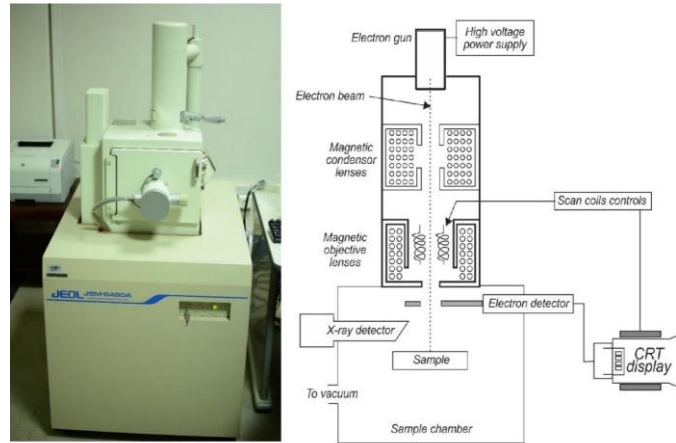


Figure 3.13: JEOL JSM 6490A figure and schematic [98]

It is a strong imaging technology which produces highly resolved, 3D images of the sample's surfaces by using focused electron's beam as shown in Figure 3.13. It is widely used in many scientific and industrial domains for material characterization [98].

3.10.1 Working principle of SEM

It uses the precisely focused electron's beam to scan the specimen's surface. Interaction of the electrons with the substance produces different signals. These signals then identified and exploited to provide detailed pictures and quantitative data on the topography and composition of the sample. Schematic representation of Scanning Electron Microscopy is shown in Figure 3.14.

3.10.2 Components of a Scanning Electron Microscope

Source of Electron: It is usually a tungsten filament or field emission gun, which emits electrons when heated.

Electron Lenses: Focus and regulate the electron beam.

Specimen Stage: Holds the sample and allows for accurate positioning.

Detectors: Gather various signals emitted from the sample.

Imaging System: Converts signals into images that are displayed on a monitor.

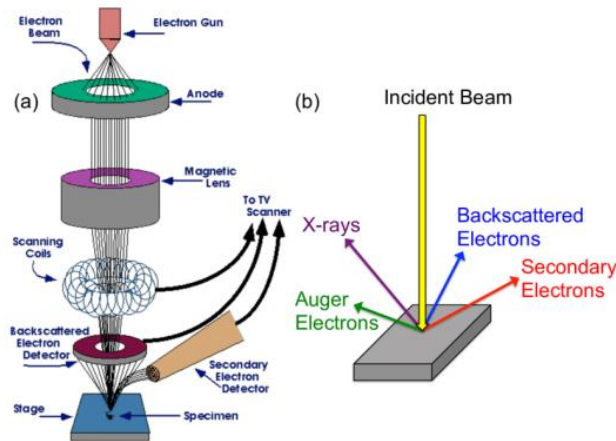


Figure 3.14: Schematic drawing of Scanning Electron Microscope [99]

3.10.3 Types of Imaging in SEM

Secondary Electron Imaging (SEI): This technique provides detailed topographical information, focusing on surface features.

Backscattered Electron Imaging (BEI): Provides information about compositional differences by reflecting the atomic number of the substance.

X-ray Analysis: Elemental analysis based on the sample's characteristic X-rays.

3.10.4 Applications of Scanning Electron Microscopy

Material Science: Study of the properties of substances such as ceramics, metals, polymers and composites.

Biology: Photographing biological specimens such as cells, tissues, and microbes.

Geology: Study of minerals and other geological samples.

Nanotechnology: Characterization of nanoparticles and nanostructures.

Forensics: Examining forensic evidence, such as fibers, hairs, and gunshot residues [99].

3.11 Energy Dispersive X-ray Spectroscopy (EDX or EDS)



Figure 3.15: EDX measurement inside the SEM [100]

It is a method that is utilized to identify element of materials and it is typically combined with the SEM as shown in Figure 3.15, to offer information about the composition of samples at the microscale.

3.11.1 Working principle of EDX

EDS depends on high-energy electrons interacting with atoms in a sample. When the primary beam of electrons incident on sample, inner shell electrons are removed. Higher energy electrons subsequently fall into these vacancies, generating distinctive X-rays in the process. These X-ray energies are typical of the elements involved, allowing identification and quantification [100]. EDX set-up is shown in Figure 3.16

3.11.2 Components of an EDX System

Detector: Determines the X-rays's energies that emits out of the sample.

Pulse Processor: Converts the electrical signals of the detector into digital signals.

Multichannel Analyzer (MCA): Sorts and records the X-ray signals according to their energies.

Software: Analyzes the X-ray spectrum and gives elemental composition information.

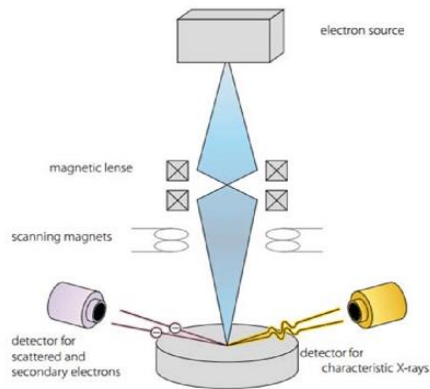


Figure 3.16: EDX Set-up [101]

3.11.3 Key Features of EDX

Elemental Identification: This method provides information about elements of a sample.

Spatial Resolution: When combined with SEM, it is possible to analyse specific regions at the microscale.

Surface Sensitivity: Provides information on a material's surface composition.

3.11.4 Applications of EDX

Material Characterization: Identification of elements in different materials such as minerals, metals, and biological substances.

Geology: Study of the mineral compositions of geological samples.

Metallurgy: Metal alloy quality control and analysis.

Nanotechnology: Characterization of nanoparticles and nanomaterials.

Biology and Medicine: Investigation of biological samples and tissues [101].

3.12 Raman Spectroscopy

It is a strong analytical chemistry method for studying modes of vibration, modes of rotation, and other modes of less frequency in a solution. It depends upon the Raman phenomenon, which was discovered in 1928 by C.V. Raman. Raman spectroscopy can be used to identify and characterize chemical substances by providing information on molecular vibrations. [102].

3.12.1 Principle of Raman Spectroscopy

When monochromatic beam of light (typically laser light) interacts with the material, the scattered beam undergoes a frequency shift due to the interaction with molecular vibrations. The scattered light has both the incident frequency (Rayleigh scattering) and frequencies shifted by the molecules having vibrational modes in the sample (Raman scattering). Schematic illustration of Raman spectrometer is represented in Figure 3.17.

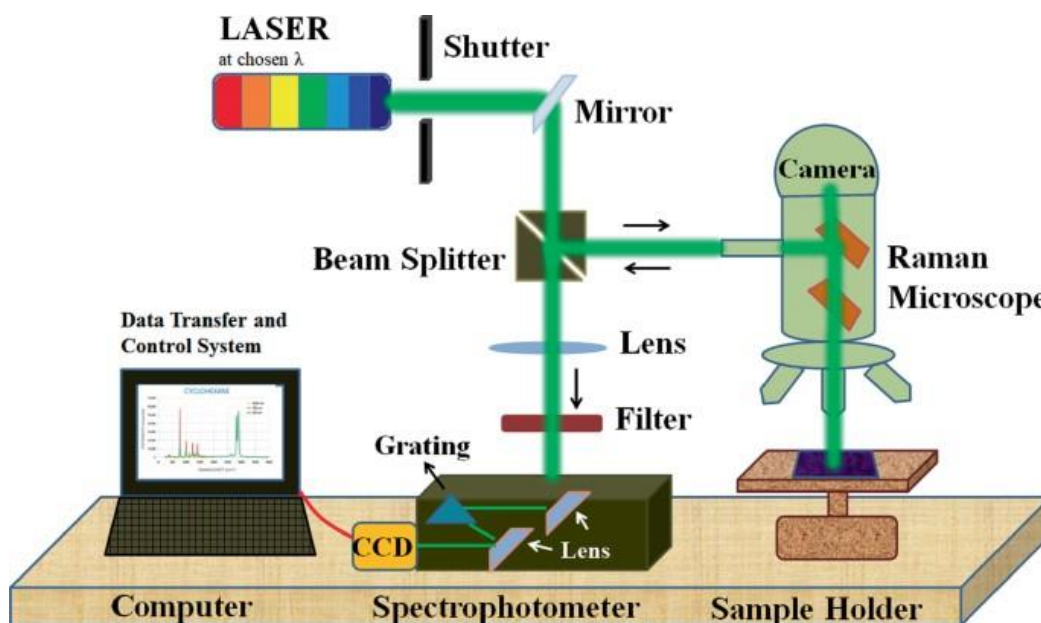


Figure 3.17: Schematic illustration of Raman spectrometer [103]

3.12.2 Parts of a Raman Spectrometer

Light Source: It is monochromatic and collimated light source, typically in the visible or near-infrared regions.

Sample: Material under investigation.

Monochromator: Separates scattered light into its different wavelengths, allows the detection of Raman-shifted frequencies.

Detector: Measures the strength of the scattered light from various wavelengths.

Analyzer: Optional, used for the filtration of unwanted wavelengths [103].

3.12.3 Raman Spectroscopy Modes

Stokes Scattering: The most common type of scattering, in which the dispersed light has less energy (a longer wavelength) than the incident light.

Anti-Stokes Scattering: It occurs when scattered light has more energy (a shorter wavelength) than incident light. Because of the reduced chance, this is less common. Raman scatterings are shown in Figure 3.18.

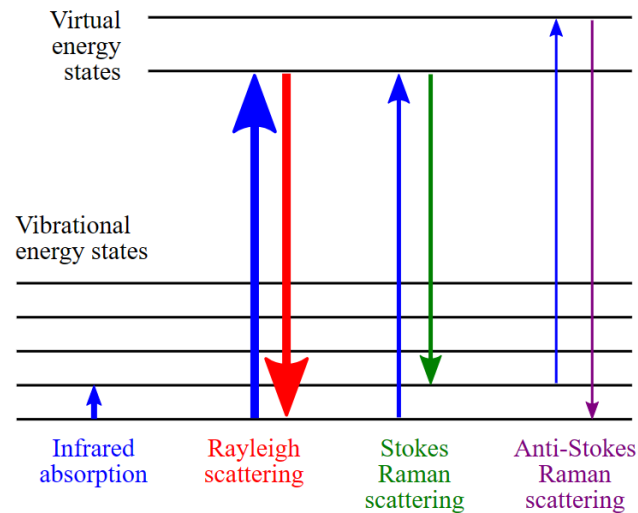


Figure 3.18: Raman Scatterings [104]

3.12.4 Applications of Raman Spectroscopy

Chemical Analysis: Identification of chemical compounds in variety of domains, such as pharmaceuticals, forensics, and environmental analysis.

Material Science: Study of properties of materials, such as polymers, ceramics, and composites.

Biomedical Applications: Detection and analysis of biological molecules, tissues, and cells.

Environmental Monitoring: Identification of pollutants as well as monitoring of environmental samples.

Quality Control: Used in industries such as food and beverage, to identify and quantify components in a sample [104].

3.13 Photoluminescence Spectroscopy (PL)

PL spectroscopy is a strong analytical method used to investigate emission of light from a substance after photon absorption. This method is frequently used in a variety of domains, including materials science, semiconductor physics, and biology. PL spectroscopy can give useful information about optical and electrical properties of materials [105]. PL spectrometer is shown in Figure 3.19. PL emission spectrum is mostly utilized for the investigation of charge carrier's trapping, migration, and transport's efficiency to determine destiny of electron and hole pairs. Emissions of PL is mostly caused by the excited electron and hole pair's recombination.

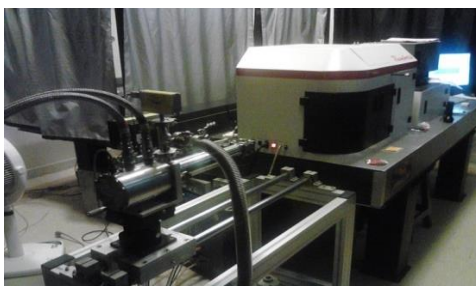


Figure 3.19: PL Spectrometer [105]

3.13.1 Principle of PL Spectroscopy

Photoluminescence happens when a material absorbs photons from a light source, often a laser. Whenever the material receives energy of the external sources, electrons can get stimulated and transported high energy levels from ground state. However, the electrons get de-excited since they do not not stable at higher energies states and emits light at longer wavelengths. This emitted light can be detected and analyzed to learn more about the material's electrical and optical properties [105]. Experimental setup of PL is shown in Figure 3.20.

3.13.2 Components of a PL Setup

Light Source: Gives photons to excite the sample. Common sources are lasers or other intense light sources.

Sample Holder: Holds the sample to be analyzed.

Monochromator: It selects specific wavelengths of emitted light for analysis

Detector: Measures the intensity of the emitted light [106].

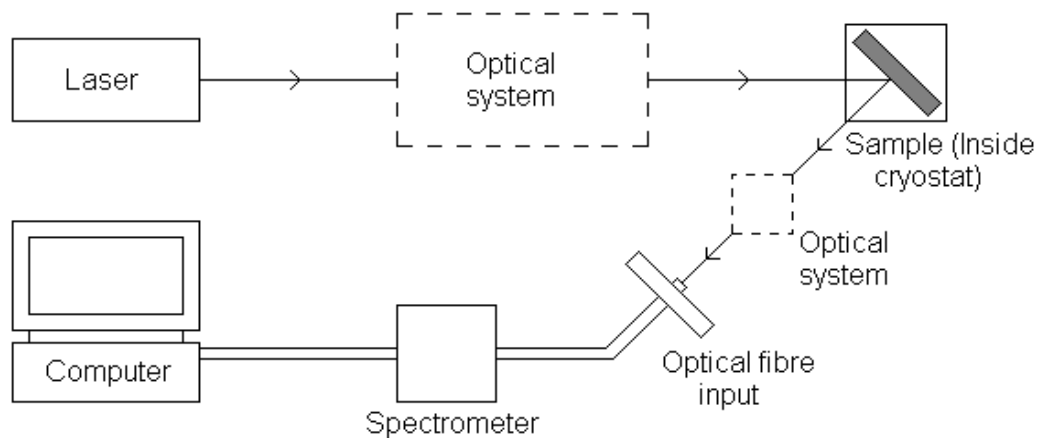


Figure 3.20: Experimental setup of PL [106]

3.13.3 Types of Photoluminescence

Fluorescence: The material absorbs photons and rapidly re-emits light.

Phosphorescence: The material absorbs photons and then re-emits light after a delay, which is often caused by a longer-lived excited state. Absorption and emission paths of photons are shown in Figure 3.21

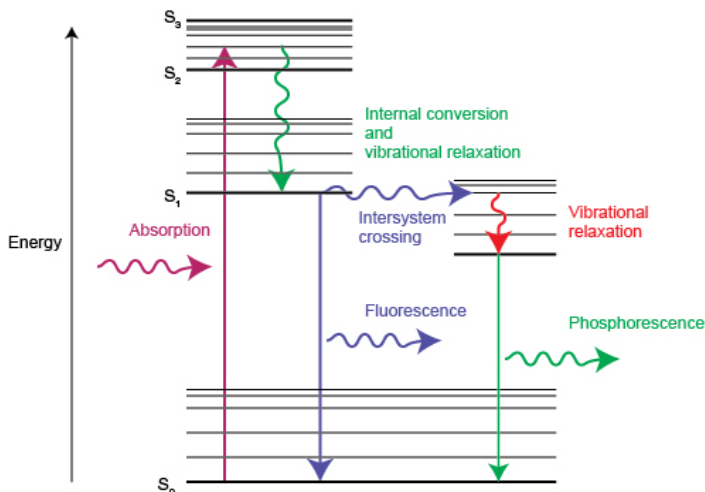


Figure 3.21: Absorption and emission paths of photon [107]

3.13.4 Applications of PL Spectroscopy

Semiconductor Characterization: Studying the semiconductors and electronic properties of quantum dots.

Material Science: Analyzing the properties of luminescent materials like phosphors and nanoparticles.

Biology and Medicine: Using fluorescent dyes and proteins to investigate cellular processes and biomarkers.

Nanotechnology: Study the optical properties of nanomaterials.

Solar cells: Evaluating the efficiency and performance of photovoltaic materials [107].

3.14 DSSCs characterization (IV)

When a solar cell is shined by light, photo-current is generated due to transition of electrons from HOMO to LUMO, that generated charge carrier flows through the external circuit, contributing to the V and I of the curve of solar cell, which is called the characteristic IV curve as shown in Figure 3.22 [108].

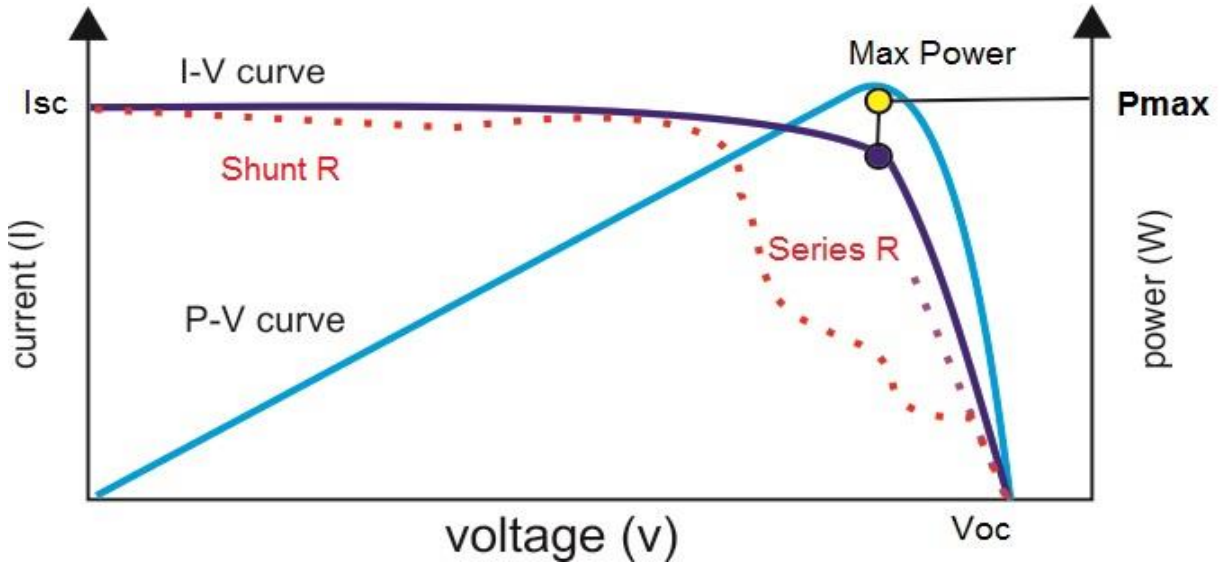


Figure 3.22: Characteristic curve of solar cell [108]

3.14.1 Solar cells characteristics parameters

The maximum operating voltage is referred to as open-circuit voltage (V_{oc}), and maximum reverse current is referred as short-circuit current (I_{sc}).

This IV curve of solar cell illustrates open-circuit voltage (V_{oc}), fill-factor (FF), short-circuit current (I_{sc}) and the maximum power (P_{max}).

FF graphically represents "squareness" of IV curve. Another critical characteristic is the photo-conversion efficiency (PCE) of cells. It is solar cell's P_{in}/P_{max} ratio. The high PCE reflects the solar cell's strong performance [25].

Normally solar cells's parameters are determined under AM 1.5 solar irradiance at 25 °C temperature. Efficiency can be derived by following equation:

$$\eta = \frac{P_{max}}{P_{in}} = \frac{FF J_{SC} V_{oc}}{P_{in}}$$

In this research, A Keithley 2400 source metre connected to a PC was used to calculate current-voltage (J-V) for DSSCs.

CHAPTER 4: RESULTS AND DISCUSSION

4.1 Current-time curve

Figure 4.1 shows the current-time curves obtained during the two-step anodization of Ti. Both steps displayed similar current-time behavior but with varying current densities. The first step curve shows a dramatic drop in current at the start of the anodization process due to the creation of a barrier oxide layer. This drop in current was followed by an increase in current due to oxide layer pitting by fluoride ions, after which the current was stabilized. The current density was higher in the second step compared to that in the first one. This phenomenon can be explained by the following factors: Firstly, the reduction in current within the first 10 seconds was 1 % less in the second step than that in the first one. This is because pore nucleation is significantly faster in second step anodization than in first step anodization because the nanopits of the textured titanium surface generated by first step anodization and the removal of oxide encourage the nucleation of tubes. [86].

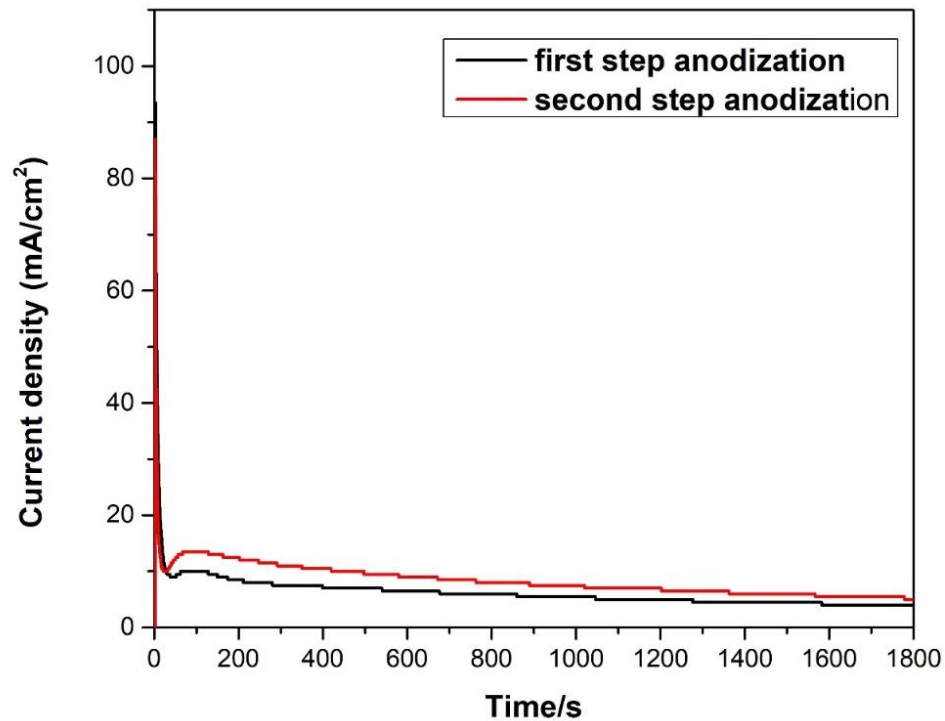


Figure 4.1: Current-time plots during the first- and second-step anodization of Ti.

Hence a thinner barrier oxide layer was produced in the second step due to the pre-existing oxide layer on the Ti prior to treatment; The thickness of the barrier oxide layer determines the electrode's resistance and hence, its current density. Secondly, in the second step, the electric field has a regular distribution because of the highly ordered surface, which helps in raising the current density [109].

4.2 Morphological and elemental analysis

4.2.1 Scanning Electron Microscopy

The morphologies of the samples were analyzed using scanning electron microscopy (SEM) TESCAN, MAIA3 TriglavTM with accelerated voltage of 20 KV. The SEM images of open and grassy TiNTs are shown in Figure 4.1 (a, b). Figure 4.2(a) shows that the top surface of open TiNTs is ordered and homogeneous. Figure 4.2(b) depicts a grassy TiNTs array made up of two layers of oxide: a nanograss layer with a disordered morphology and an ordered nanotubes layer beneath the nanograss layer. Nanograss is generated by the persistent etching of the tube walls in the fluoride-containing electrolyte [110].

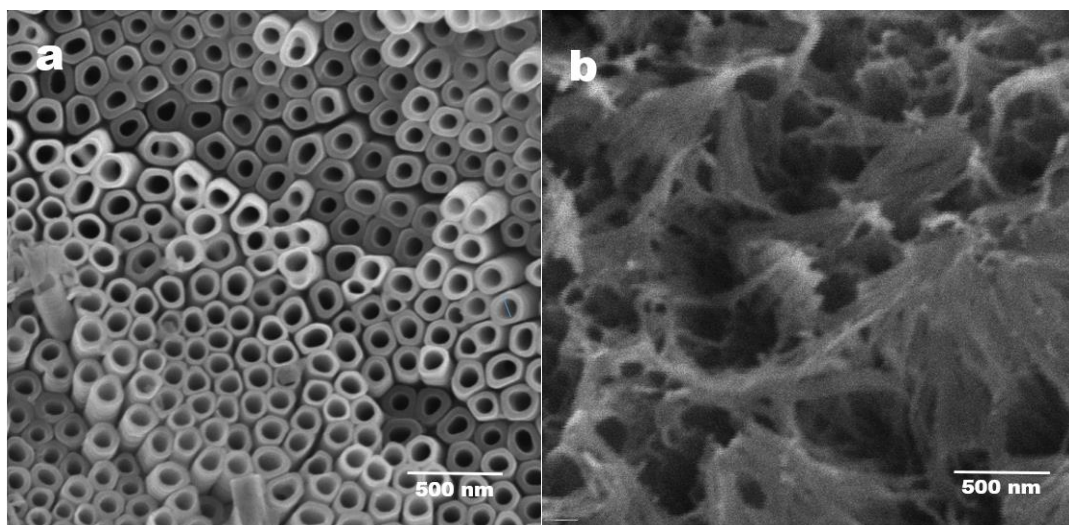
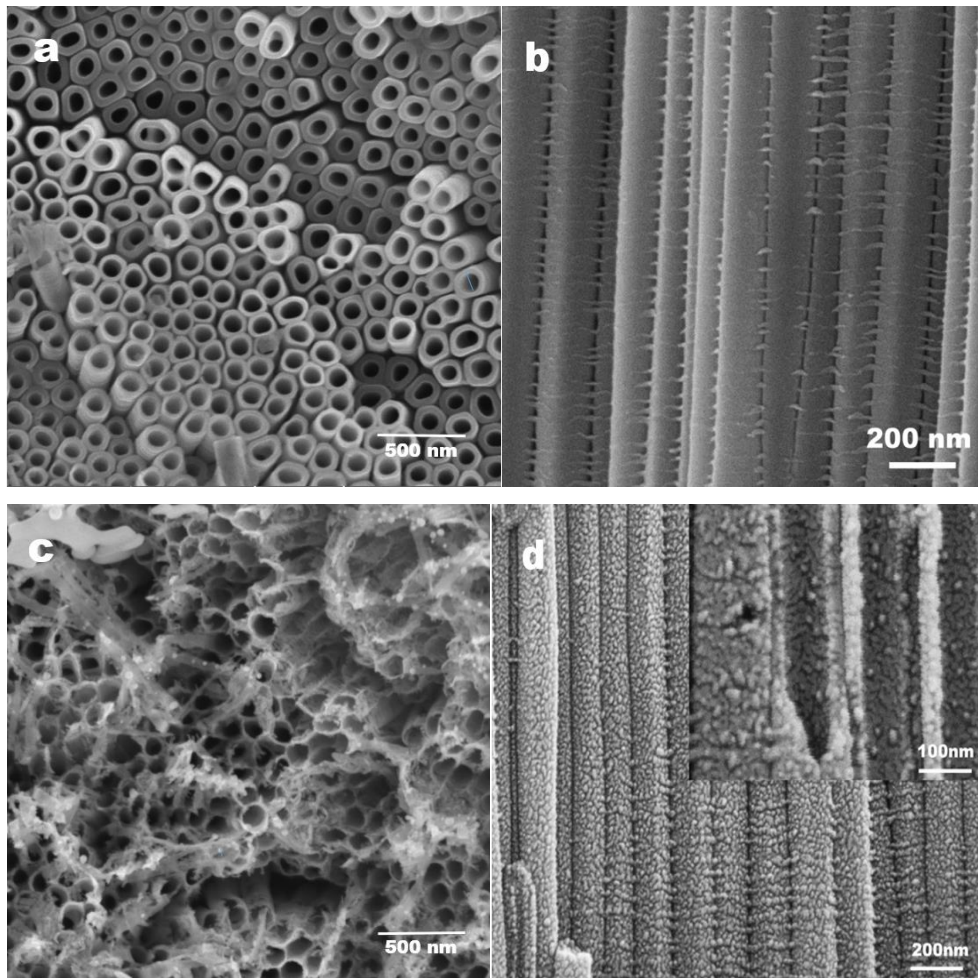


Figure 4.2: SEM images of open (a) and grassy TiNTs (b).

Top-view images of open TiNTs and AgNPs/TiNTs at 10 (10-AgNPs/TiNTs), 15 (15-AgNPs/TiNTs), and 25 mA/cm² (25-AgNPs/TiNTs) pulse currents with 1s/ 3s on/off

time in 100 deposition cycles are shown in Figure 4.3(a)-(f). Figure 4.3(a) shows that the top surface of open TiNTs was relatively ordered and homogeneous, with an average external diameter of 0.2 μm , internal diameter of 0.1 μm , wall thickness of 0.1 μm and film thickness of 6 μm . Figure 4.3(b) demonstrates cross-section view of open TiNTs showing vertical alignment of the tubes. Through the pulse current deposition, AgNPs with different sizes were dispersed uniformly and well deposited on the top surface as well as wall of the open TiNTs as shown in Figure 4.3(c)-(f). These particles are spherical in shape with different sizes at different pulse currents. At 10 mA/cm^2 pulse current, Figure 4.3(c, d) AgNPs are well deposited with the mean size of 25 nm. At 15 mA/cm^2 pulse current, Figure 4.3(e), particle size of AgNPs increased to a value of 162 nm. At 25 mA/cm^2 pulse current, Figure 4.3 (f), there is a large agglomeration of AgNPs with mean size of 169 nm. The size ranges of AgNPs produced at various pulse currents are listed in Table 4.1. These results showed that the size of AgNPs on open TiNTs increases with the increase in pulse current.



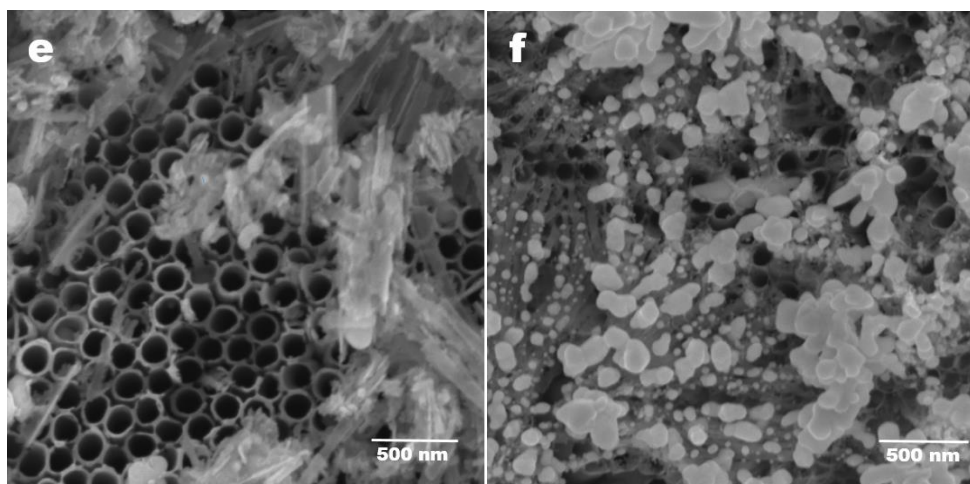


Figure 4.3: SEM images of open TiNTs (a, b) and AgNPs/open TiNTs obtained at different pulse currents: (c, d) 10 mA/cm², (e) 15 mA/cm², and (f) 25 mA/cm².

Table 4.1: Effect of pulse current density on size of AgNPs.

Sample	Composition	Pulse current mA/cm ²	Estimated diameter of Ag particle (nm)
Open TiNTs	TiO ₂	-	-
10-AgNPs/open TiNTs	Ag/ TiO ₂	10	12-41
15-AgNPs/open TiNTs	Ag/ TiO ₂	15	41-284
25- AgNPs/open TiNTs	Ag/ TiO ₂	25	132-206

Figure 4.4(a)-(c) shows the top-view images of AgNPs/grassy TiNTs at 10mA/cm² (10-AgNPs/grassy TiNTs), 15mA/cm² (15-AgNPs/grassy TiNTs), and 25 mA/cm² (25-AgNPs/grassy TiNTs) pulse currents with 1s/ 3s on/off time in 100 deposition cycles.

Through the pulse current deposition, AgNPs are dispersed on grassy TiNTs at different pulse currents. Figure 4.4(a)-(c) shows that Ag NPs have non-homogeneous dispersion on grassy TiNTs and deposition of Ag NPs increases with increasing pulse current on grassy TiNTs.

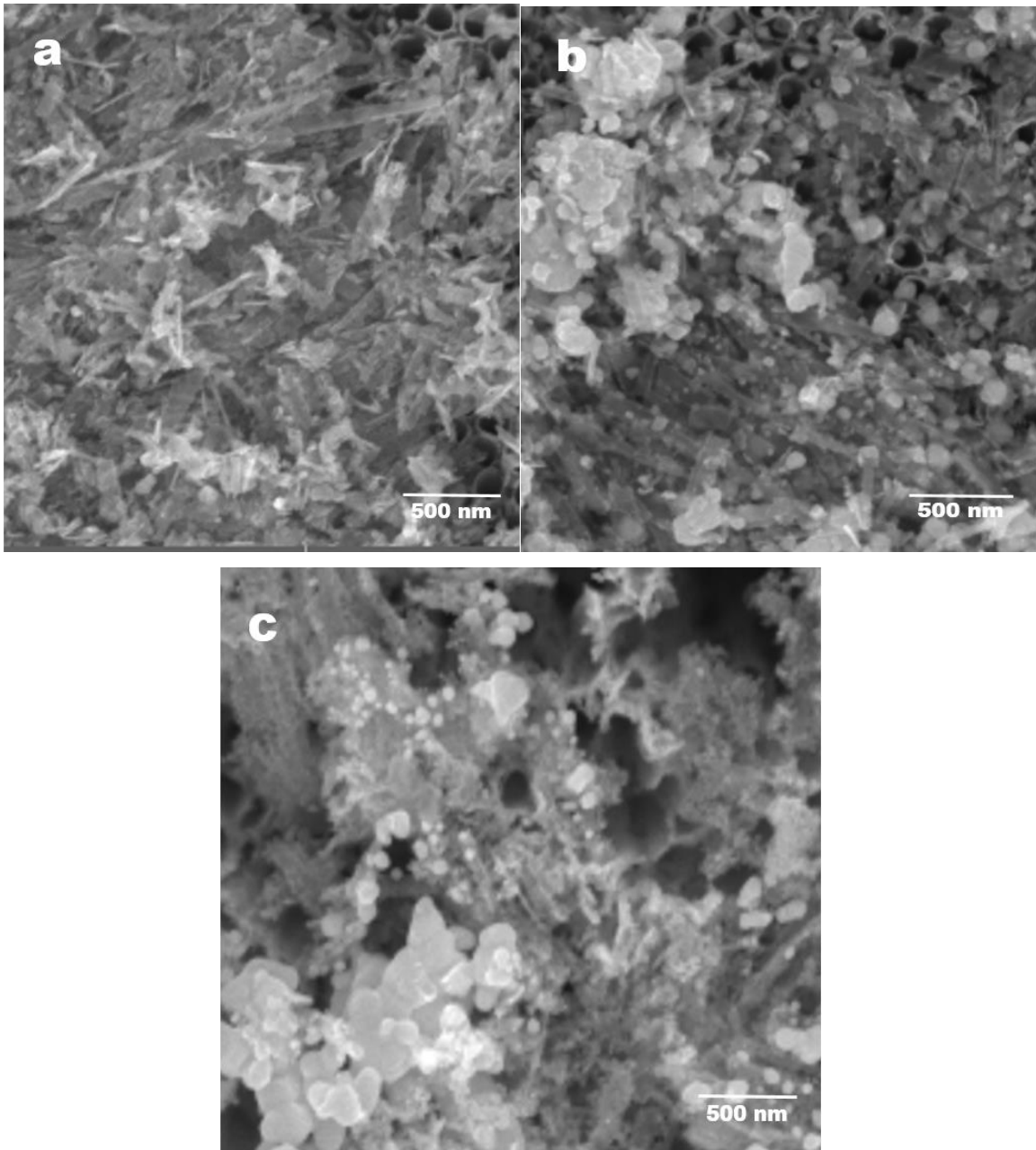


Figure 4.4: SEM images of AgNPs/grassy TiNTs obtained at different pulse currents: (a) 10 mA/cm², (b) 15 mA/cm² and (c) 25 mA/cm².

4.2.2 Energy Dispersive X-ray Spectroscopy

Energy-Dispersive X-ray Spectroscopy (EDX) was used to analyze the elemental composition of TiNTs.

The EDX spectrums of open and grassy TiNTs are shown in Figure 4.5(a, b) and the chemical compositions are given in the inset. In the EDX spectrum of both open and grassy TiNTs there are peaks of Ti and O which confirms the presence of these elements in both samples.

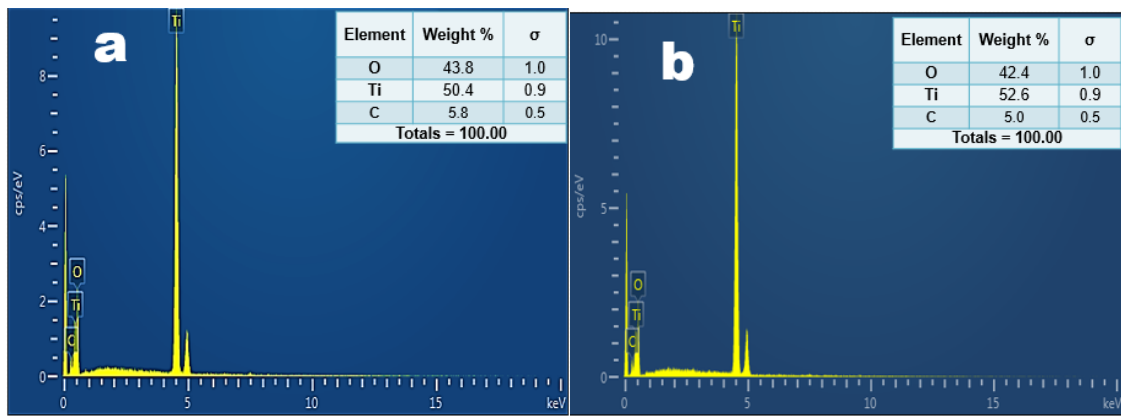


Figure 4.5: EDX patterns of open (a) and grassy TiNTs (b).

The EDX spectrums of bare open TiNTs and open TiNTs decorated with AgNPs are given in Figure 4.6(a)-(d) with % age compositions in the insets. In the EDX spectrum of bare TiO_2 , Figure 4.6(a) there are peaks of Ti and O which confirms the presence of these elements in the sample.

At 10 mA/cm^2 pulse current, Figure 4.6(b) there was an additional peak of Ag with weight% of 5.5. At 15 mA/cm^2 pulse current, Figure 4.6(c) weight% of Ag increased to a value of 12.3.

The weight% of Ag was further increased to 23.8 when the pulse current density was raised to 25 mA/cm^2 , Figure 4.6(d). Thus, the EDX results confirmed the presence of AgNPs at the TiNTs and that the deposition of AgNPs on the TiNTs increased with increasing pulse currents.

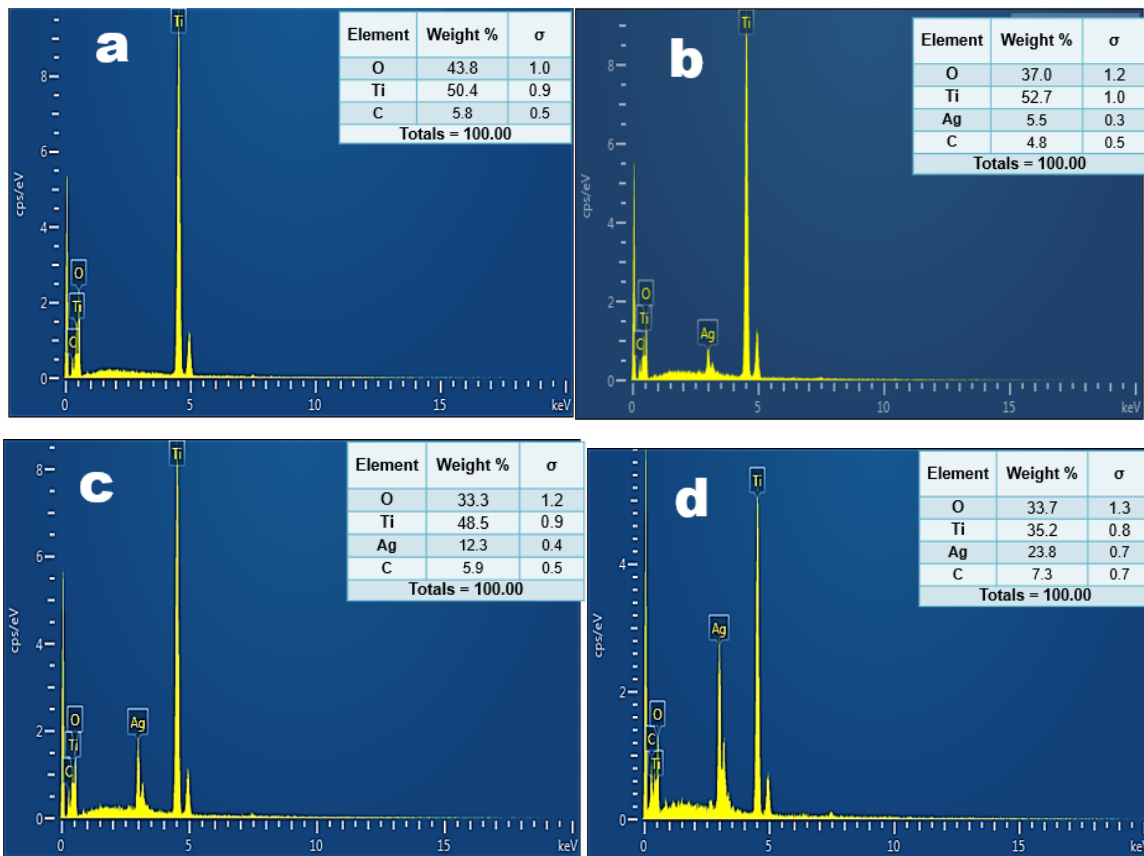


Figure 4.6: EDX patterns of (a) open TiNTs, (b) 10-AgNPs/open TiNTs, (c) 15-AgNPs/open TiNTs, (d) 25-AgNPs/open TiNTs.

Figure 4.7(a)-(c) shows the EDX spectrums of AgNPs/grassy TiNTs at various pulse currents, with chemical compositions provided in the inset. Ti and O peaks appear in the EDX spectrums, indicating the existence of these elements. At 10 mA/cm² pulse current, Figure 4.7(a) shows an additional peak of Ag with a weight % of 6.8. At a pulse current of 15 mA/cm², Figure 4.7(b) shows that the weight % of Ag is 16.1.

At a pulse current of 25 mA/cm², Figure 4.7(c) shows that the weight % of Ag is 26.7. As a result, the EDX spectra confirmed the creation and existence of AgNPs on grassy TiNTs at various pulse currents. The results confirmed that the deposition of AgNPs on the TiNTs increases with increasing pulse currents. Also, the EDX results show that grassy TiNTs have more deposition of Ag NPs as compared to open TiNTs at different pulse currents.

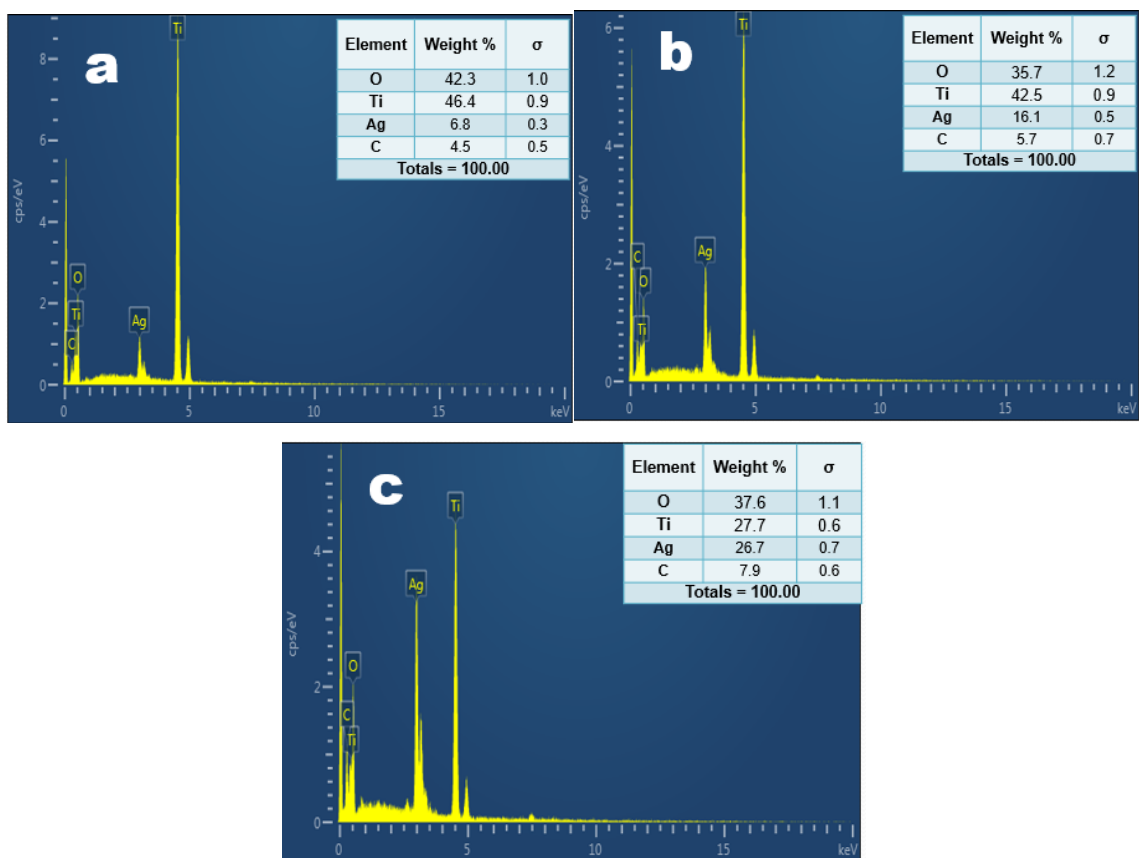


Figure 4.7: EDX patterns of (a) 10-AgNPs/grassy TiNTs, (b) 15-AgNPs/grassy TiNTs, (c) 25-AgNPs/grassy TiNTs.

4.3 Structural analysis

4.3.1 X-ray diffraction (XRD)

The XRD patterns were acquired on ARL Equinox 3000 using $\text{CuK}\alpha$ radiation. The X-Ray tube voltage was 40 KV with 40 mA current. Figure 4.8 shows the XRD patterns of open and grassy TiNTs. The samples were vacuum-annealed at 450°C for two hours, and the pattern clearly showed that the prepared TiNTs exhibited characteristic diffraction peaks that were well matched with the standard pattern of JCPDS (01-084-1286) of anatase TiO_2 crystals [111]. The peaks of Ti are because of the Ti substrate of samples (JCPDS card No. 44-1294) [55]. XRD patterns also confirm the presence of TiO_2 in these samples.

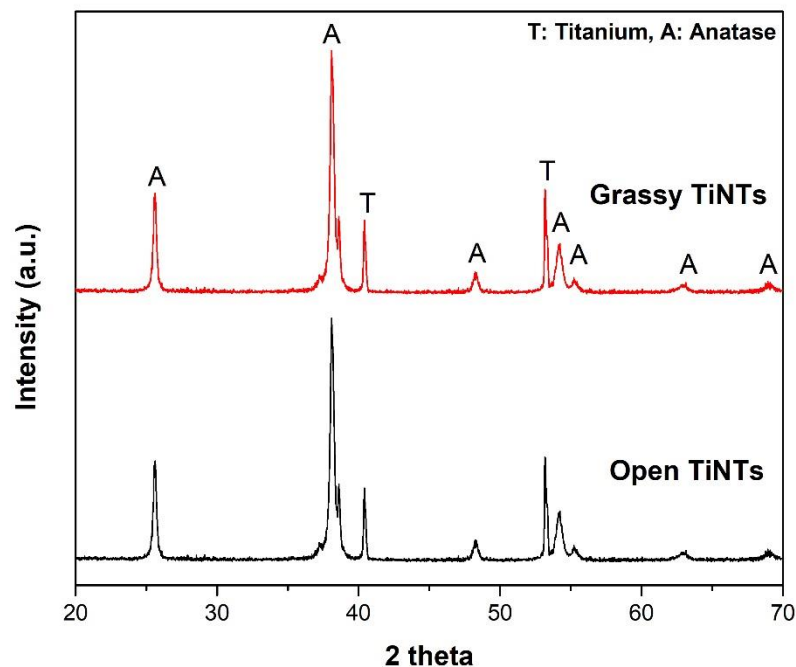


Figure 4.8: XRD patterns of open and grassy TiNTs.

Figure 4.9 shows the XRD patterns of open TiNTs and TiNTs loaded with AgNPs. The samples were vacuum annealed at 450°C for two hours before XRD studies. XRD pattern of TiO₂ nanotube arrays exhibited typical diffraction peaks which were well matched with the standard JCPDS card number (01-084-1286) showing the anatase phase of TiO₂ [111]. Metallic phase (JCPDS card No. 44-1294) [55] of Ti was resulted from the non-anodized substrate. The anatase phase of TiO₂ remained unchanged after the deposition of Ag NPs on to the TiO₂ nanotubes. The XRD spectra of 15-AgNPs/TiNTs and 25-AgNPs/TiNTs showed additional peaks at 2 θ angles of = 44.50 and 64.60 corresponding to the (200) and (220) planes of metallic Ag, respectively (JCPDS card No. 04-0783) [112]. The TiO₂ anatase peaks at 37.80 (004) and 38.60 (112) overlap with the Ag (111) peak at 38.10, making it difficult to see clearly. However, no silver peaks were seen in the sample of 10-AgNPs/TiNTs composite at a pulse current of 10 mA/cm². This is most likely because of the low silver content, which is not detectable using XRD methods. XRD patterns revealed the successful synthesis of Ag nanoparticles on TiNTs.

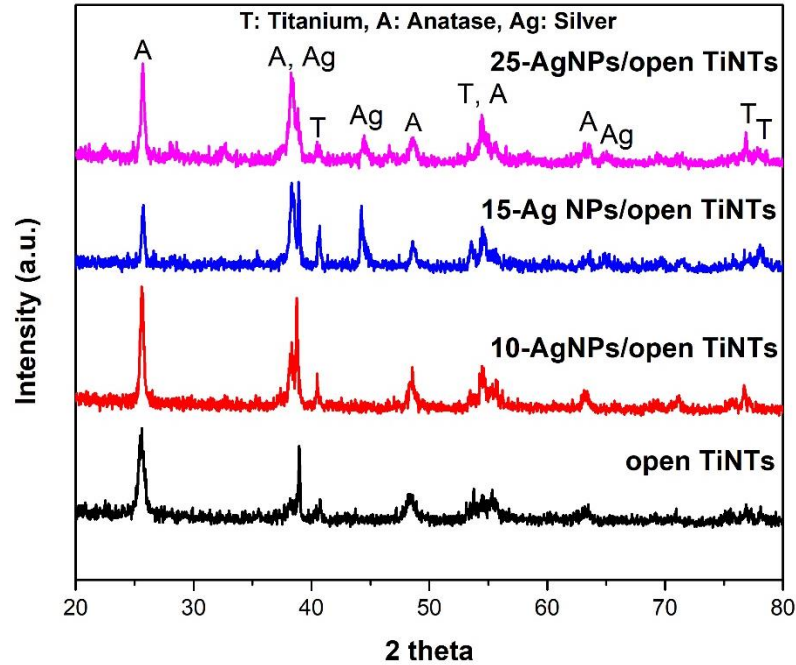


Figure 4.9: XRD patterns of open TiNTs and AgNPs/open TiNTs at 10, 15 and 25 mA/cm² pulse currents.

Figure 4.10 depicts the XRD patterns of AgNPs/grassy TiNTs at various pulse currents. The pattern clearly reveals that the created TiNTs had typical diffraction peaks that were well matched with the standard pattern of JCPDS (01-084-1286) of anatase TiO₂ crystals. [111]. The metal Ti phase peaks are because of the Ti substrate of samples (JCPDS card No. 44-1294) [55]. The TiO₂ diffraction band remained unchanged after the deposition of Ag NPs on the grassy TiNTs.

The XRD spectra of 15-AgNPs/TiNTs and 25-AgNPs/TiNTs revealed additional bands at $2\theta = 64.60$, which correspond to the face bands of Ag (220), respectively (JCPDS card No. 04-0783) [112]. However, no such peak was observed in 10-AgNPs/grassy TiNTs, this might be due to the low silver amount in grassy TiNTs at 10 mA/cm² pulse current. The TiO₂ anatase peaks at 37.80 (004) and 38.60 (112) overlap with the Ag (111) peak at 38.10, making them difficult to distinguish. Also, the peak of Ti at $2\theta = 44.50$ is overlapping with the face band of Ag (200). XRD patterns of grassy samples also confirmed the existence of Ag nanoparticles on grassy TiNTs.

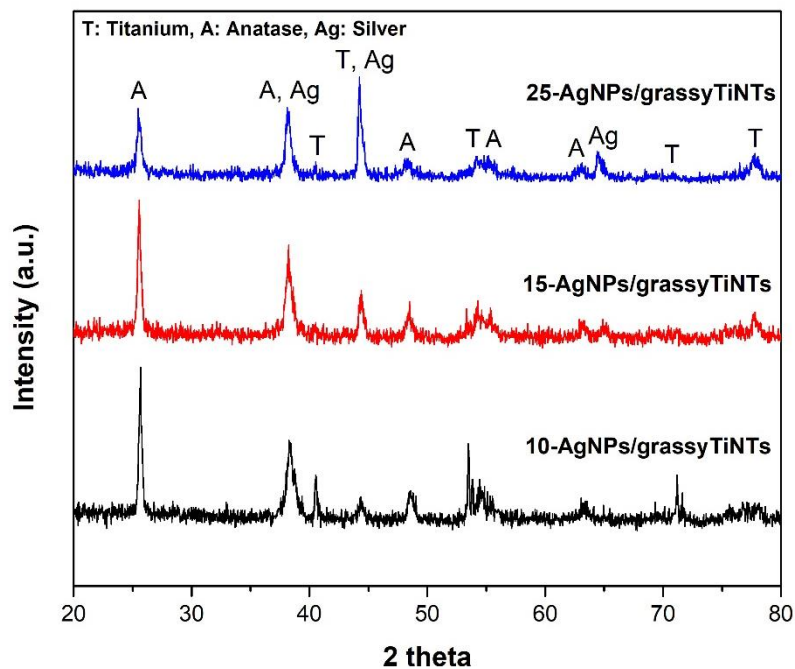


Figure 4.10: XRD patterns of AgNPs/grassyTiNTs at 10, 15 and 25 mA/cm² pulse currents.

4.3.2 Raman Spectroscopy

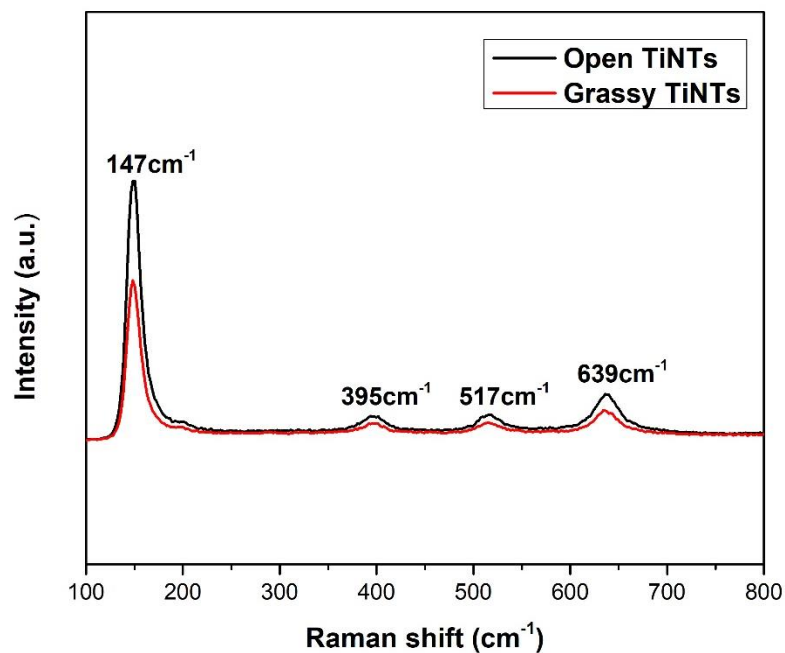


Figure 4.11: Raman spectra of open and grassy TiNTs.

Raman spectroscopy was performed to better understand the structure of the prepared TiNTs. Raman spectra were acquired on a Micro Ramboss Dongwoo optron spectrometer Figure 4.11 shows the Raman spectra of open and grassy TiNTs. The major Raman bands in all of the samples are due to the characteristic anatase phase of TiO_2 , which is characterized by the bands at 147 cm^{-1} , 395 cm^{-1} , 517 cm^{-1} , and 639 cm^{-1} [59]. However, the Raman intensity of the bands relevant to grassy TiNTs is less as compared to open TiNTs. This variation in intensity might be due to the grass that effects the resonant Raman signal of TiO_2 in grassy TiNTs.

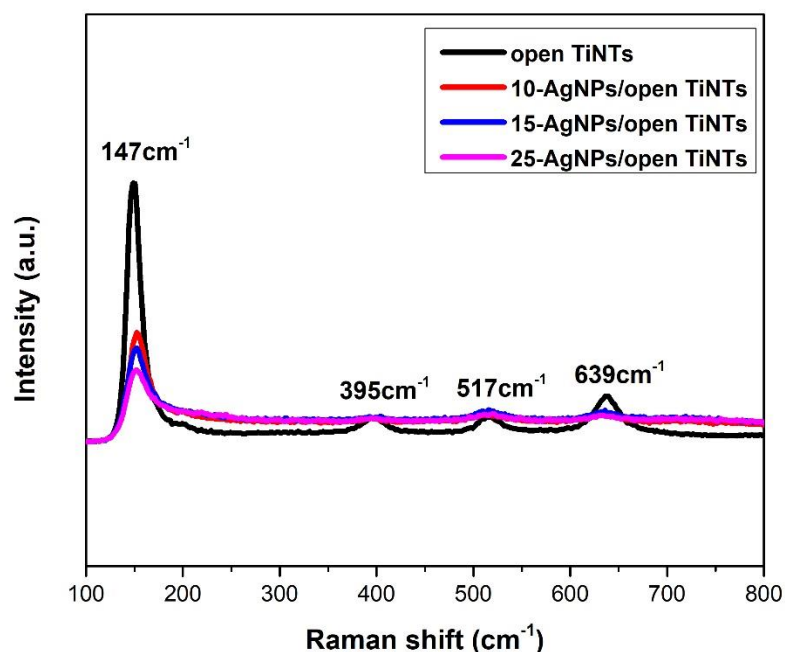


Figure 4.12: Raman spectra of open TiNTs and AgNPs/open TiNTs at 10, 15 and 25 mA/cm^2 pulse currents.

Figure 4.12 depicts the Raman spectra of open TiNTs and AgNPs/open TiNTs at pulse currents of 10, 15, and 25 mA/cm^2 . The predominant Raman bands in all of the samples are assigned to the characteristic anatase phase for TiO_2 , which is characterized by the bands at 147 cm^{-1} , 395 cm^{-1} , 517 cm^{-1} , and 639 cm^{-1} [59]. The Raman spectra of the AgNPs/TiNTs samples did not show any signals associated with Ag nanoparticles, which can be attributed to the low amount of Ag loaded onto TiO_2 nanotubes. However, the intensity of the bands relevant to TiO_2 decreases with increasing Ag amount (increasing

pulse current), implying that there is an interaction between Ag and TiO₂ after Ag deposition on open TiNTs, influencing the resonant Raman effect for TiO₂ [113]. Furthermore, when compared to pure open TiNTs, the major peak of AgNPs/open TiNTs samples is slightly shifted, which could be attributed to the interface structure of TiO₂ and Ag [114].

Figure 4.13 shows the Raman spectra of AgNPs/grassy TiNTs at pulse currents of 10, 15, and 25 mA/cm². The major Raman bands in all of the samples are ascribed to the characteristic anatase phase of TiO₂, which is characterized by the bands at 147 cm⁻¹, 395 cm⁻¹, 517 cm⁻¹, and 639 cm⁻¹ [59]. The Raman spectra of the AgNPs/grassy TiNTs samples revealed no signals associated with Ag nanoparticles, which can be attributed to the low Ag loading onto grassy TiNTs. However, the strength of the bands relevant to TiO₂ diminishes with increasing Ag amount (increasing pulse current), indicating that there is an interaction between Ag and TiO₂ following Ag deposition on TiNTs, impacting the resonant Raman effect for TiO₂ [113].

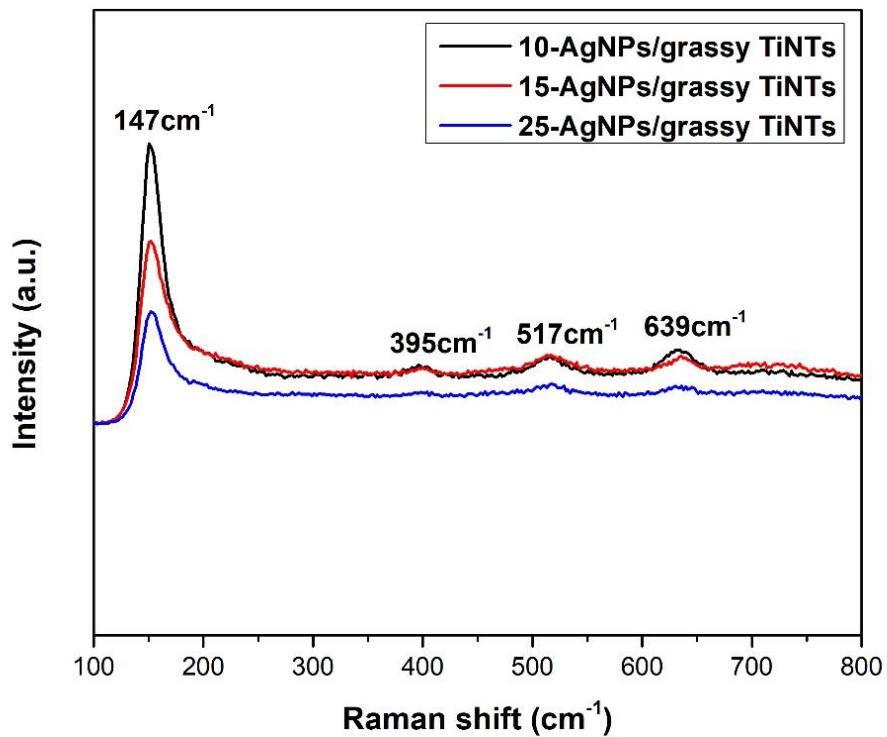


Figure 4.13: Raman spectra of AgNPs/grassy TiNTs at 10, 15 and 25 mA/cm² pulse currents.

4.4 Optical properties

4.4.1. Photoluminescence spectroscopy

Photoluminescence (PL) spectroscopy was performed to obtain information about the optical properties of the TiNTs. PL spectra were acquired on a Micro Ramboss Dongwoo oprtron spectrometer. Figure 4.14 shows the PL spectra of open and grassy TiNTs. In the PL spectra of open TiNTs, there is one prominent emission peak at roughly 380 nm, corresponding to 3.36 eV, which is ascribed to the emission of the band gap transition. [114]. There are no substantial defect-related emissions in open TiNTs, indicating the good stoichiometry and crystalline quality of the sample. [115]. The grassy TiNTs shows a broad photo-luminescence peak in the visible range at 390–450 nm or 2.7–3.1 eV. This peak corresponds to the intra-bandgap defect states in TiO₂ that emit at visible wavelengths, while no such peak was observed in open TiNTs [116]. This means that grass has affected the stoichiometry and crystallographic quality of TiNTs by introducing the defect states in TiO₂.

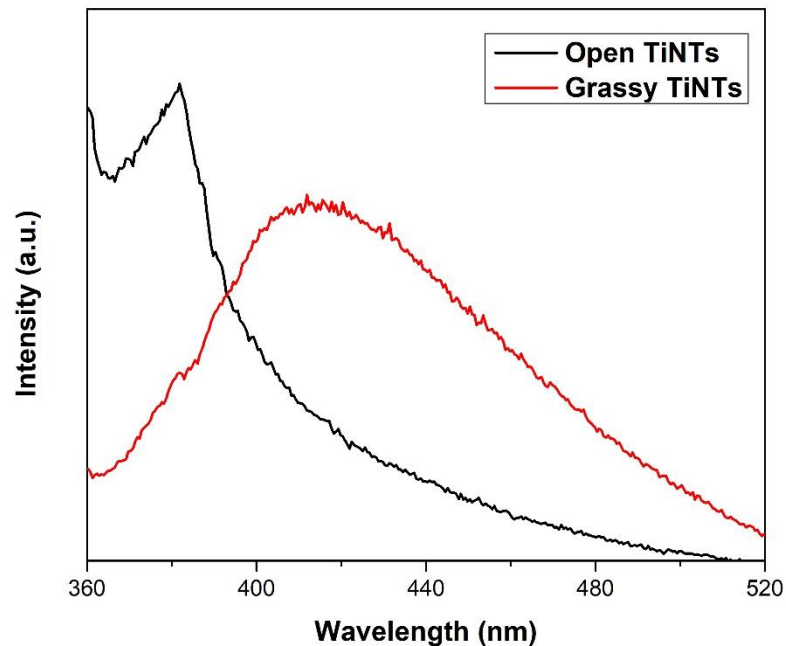


Figure 4.14: PL spectra of open and grassy TiNTs.

Figure 4.15 shows the PL spectra of open TiNTs and AgNPs/open TiNTs at pulse currents of 10, 15, and 25 mA/cm². There is one main emission peak found in the PL spectra of the produced samples in Figure 4.15, that is at around 380 nm corresponding to the 3.36 eV, which is predominantly attributed to the emission of the band gap transition [114]. Figure 4.15 shows no significant defect-related emissions, confirming the high (stoichiometry and) and crystallographic quality of samples [115]. Ag-NP decorating on open TiNTs has no qualitative effect on the morphology of the PL emission. However, the PL intensity of the Ag-NPs/open TiNTs samples was found to be substantially lower than that of the undecorated TiNTs.

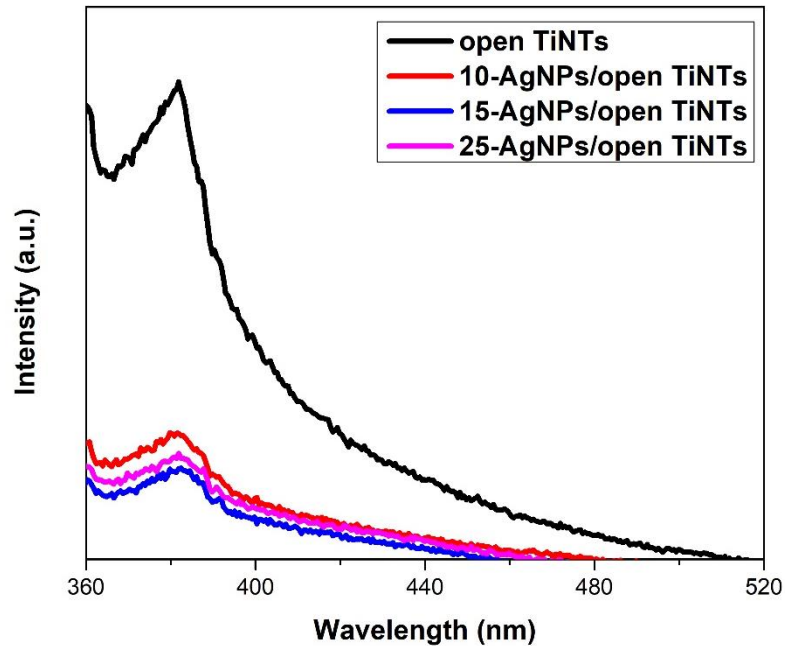


Figure 4.15: PL spectra of open TiNTs and AgNPs/open TiNTs at 10, 15 and 25 mA/cm² pulse currents.

This decrease in PL intensity shows that Ag-NPs improve the charge separation of TiNTs because of photogenerated electrons migrating from the open TiNTs conduction band to the Ag-NPs, leaving holes in the TiO₂ valence band. This effective charge separation reduces the likelihood of charge carrier recombination to produce photoluminescence, making more charges available to contribute to the photo-electrochemical production process [117]. For the AgNPs/open TiNTs samples, the PL

intensity decreased with the increasing deposition of Ag NPs from 10 to 15 mA/cm² because of the increase in charge separation and hence reduced recombination to produce photoluminescence. However, the PL intensity of TiNTs increases with increasing Ag-NPs deposition at 25 mA/cm². This increase in PL intensity of 25-AgNPs/TiNTs might be due to the increased agglomeration of Ag NPs on TiNTs which decreases the electrons migration from the TiNTs conduction band to the Ag-NPs and hence increases the recombination.

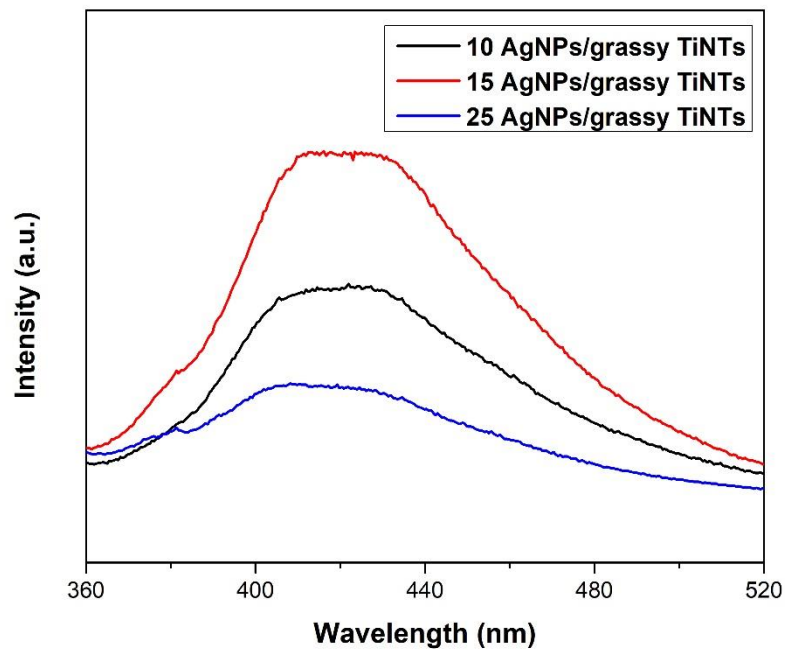


Figure 4.16: PL spectra of AgNPs/grassy TiNTs at 10, 15 and 25 mA/cm² pulse currents.

Figure 4.16 shows the PL spectra of AgNPs/grassy TiNTs at pulse currents of 10, 15, and 25 mA/cm². The prepared samples show a broad photo-luminescence peak in the visible range at 390–450 nm or 2.7–3.1 eV which corresponds to the intra-bandgap defect states in TiO₂ [116]. The PL intensity of the grassy TiNTs increases by increasing the deposition at 10 and 15 mA/cm² pulse currents. This might be due to the increased plasmonic feature of Ag NPs that could effectively transfer the photogenerated electrons to the conduction band of the TiNTs [118] that could relax in the intraband gap defect states

in TiO₂, thus increasing the PL emission. However, the PL intensity of grassy TiNTs decreases with increasing Ag NPs deposition at 25 mA/cm². This decreased in PL intensity of 25-AgNPs/grassyTiNTs might be due to the increased agglomeration of Ag NPs on grassy TiNTs and capture of holes by the large number of Ag nanoparticles itself [119]. This reduces the transfer of photo generated electrons to the conduction band of TiO₂ and hence reduces the PL intensity.

4.5 Electrical properties

4.5.1. DSSCs measurements

To evaluate the photovoltaic characteristics of pure open TiNTs and AgNPs/open TiNTs at pulse currents of 10, 15, and 25 mA/cm², a DSSC was built using each of these materials, and the assembly was illuminated under A.M. illumination at 100 mW/cm².

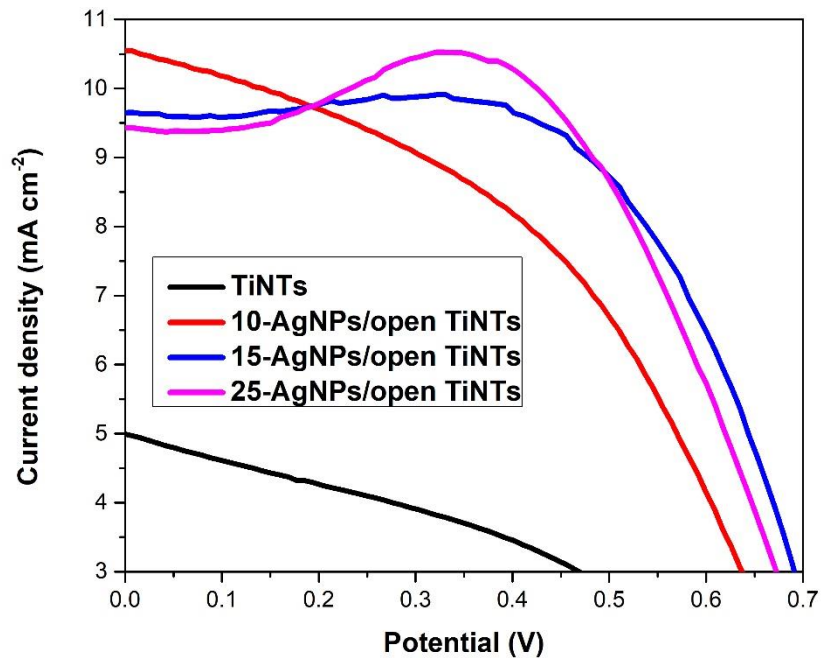


Figure 4.17: J–V curves of DSSCs fabricated using pure open TiNTs and AgNPs/open TiNTs at 10, 15 and 25 mA/cm² pulse currents.

Figure 4.17 depicts the photocurrent density-voltage (J-V) properties of cells formed with Ag NPs/open TiNTs and open TiNTs without Ag NPs. The properties of these

DSSCs are summarized in Table 4.2. Figure 4.17 shows that a photoanode made of open TiNTs without Ag NPs had the lowest short-circuit current density (J_{sc}) of 5.04 mA cm^{-2} , an open-circuit potential (V_{oc}) of 0.46 V , a fill factor (FF) of 0.39 , and a solar energy conversion efficiency (η) of 2.83% . DSSC produced with 10-AgNPs/TiNTs showed greater η of 3.59% , J_{sc} of 10.56 mA cm^{-2} , V_{oc} of 0.63 V , and FF of 0.44 compared to pure

TiNTs-based DSSC. DSSCs fabricated using 15-AgNPs/TiNTs exhibit even better properties with η of 4.46% , J_{sc} of 9.66 mA cm^{-2} , V_{oc} of 0.69 V and FF of 0.62 . DSSCs fabricated using 25-AgNPs/TiNTs exhibit lower properties as compared to 15-AgNPs/TiNTs with η of 4.32% , J_{sc} of 9.46 mA cm^{-2} , V_{oc} of 0.67 V and FF of 0.64 .

Table 4.2: Photovoltaic characteristics of dye-sensitized solar cells using pure TiNTs and AgNPs/TiNTs.

Sample	$J_{sc} \text{ (mA cm}^{-2}\text{)}$	$V_{oc} \text{ (V)}$	FF	$\eta \text{ (%)}$
TiNTs	5.04	0.46	0.39	2.83
10-AgNPs/TiNTs	10.56	0.63	0.44	3.59
15-AgNPs/TiNTs	9.66	0.69	0.62	4.46
25-AgNPs/TiNTs	9.46	0.67	0.64	4.32

This suggests that the optimum amount of AgNPs on open TiNTs can improve photoconversion efficiency. If the Ag concentration is too low, the photo-generated charge carriers are not effectively separated due to insufficient contact between them. If the amount of Ag is too high, there is an increased possibility for the capture of holes by the large number of Ag nanoparticles, excessive coverage of Ag nanoparticles on surface of TiNTs increases reflection of incident light and may also decrease photoconversion efficiency in DSSCs [119]. Figure 4.18 depicts a schematic diagram of the charge

separation and migration process in the AgNPs/open TiNTs photoanode under visible light illumination.

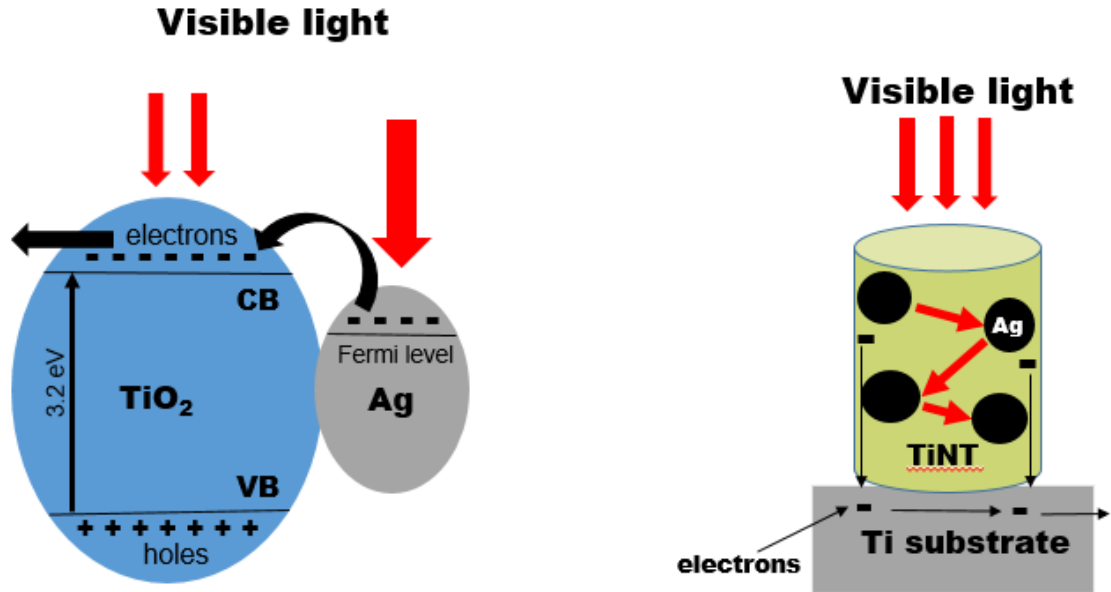


Figure 4.18: Schematic diagram for the charge separation and migration process of AgNPs/open TiNTs composite under visible light irradiation.

The grassy TiNTs coated with AgNPs by PCD method at 10, 15 and 25 mA/cm^2 pulse currents for 100 deposition cycles with 1s/3s on/off-time, were employed as photoanodes in DSSC. The JV-results of these devices are shown in Figure 4.19. Table 4.3 shows photovoltaic characteristics of dye-sensitized solar cells using AgNPs/grassyTiNTs at 10, 15 and 25 mA/cm^2 pulse currents.

Figure 4.19 shows that DSSC produced with 10-AgNPs/grassy TiNTs showed η of 2.85%, J_{sc} of 9.54 mA/cm^2 , V_{oc} of 0.61, and FF of 0.44. DSSCs fabricated using 15-AgNPs/grassyTiNTs exhibit even better properties with η of 3.62 %, J_{sc} of 10.35 mA/cm^2 , V_{oc} of 0.62 and FF of 0.49. However, by further increasing the deposition of Ag NPs on grassy TiNTs exhibit lower properties with η of 0.05 %, J_{sc} of 7.09 mA/cm^2 , V_{oc} of 0.36 and FF of 0.25.

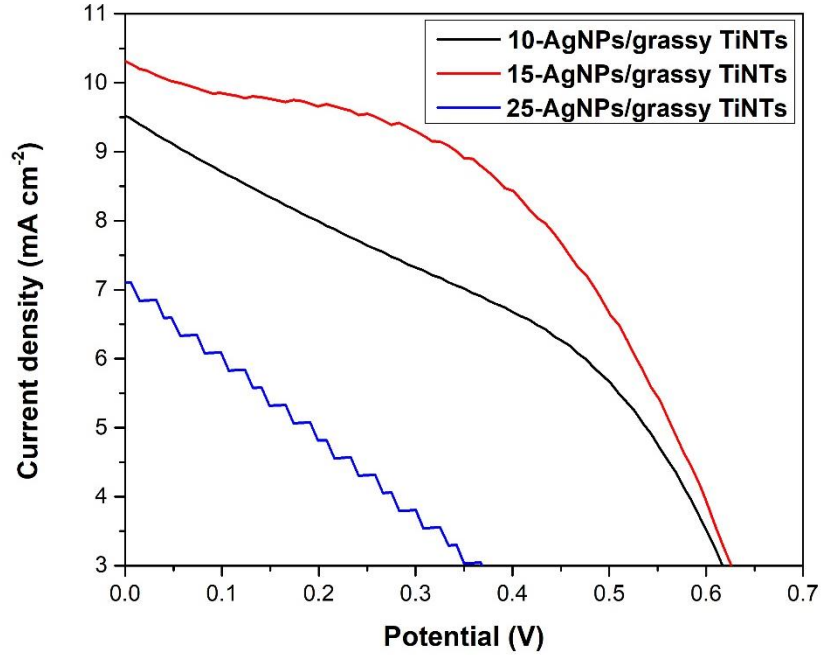


Figure 4.19: J–V curves of DSSCs fabricated using AgNPs/grassyTiNTs at 10, 15 and 25 mA/cm² pulse currents.

Table 4.3: Photovoltaic characteristics of dye-sensitized solar cells using AgNPs/grassyTiNTs at 10, 15 and 25 mA/cm² pulse currents.

Sample	J _{sc} (mA cm ⁻²)	V _{oc} (V)	FF	η (%)
10-AgNPs/grassy TiNTs	9.54	0.61	0.44	2.85
15-AgNPs/grassy TiNTs	10.35	0.62	0.49	3.62
25-AgNPs/grassy TiNTs	7.09	0.36	0.25	0.05

So, on grassy TiNTs there is also an optimum amount of AgNPs that can improve photoconversion efficiency like open TiNTs. The reason for such highly decreased in photoconversion efficiency of 25-AgNPs/grassy TiNTs might be due to the combine effect of grass and increased agglomeration of Ag NPs that decreases the charge transfer from Ag NPs to the conduction band of TiO₂ and also increased the reflection of light on grassy TiNTs [119]. Figure 4.20 depicts a schematic diagram of the charge separation and migration process in the AgNPs/grassy TiNTs photoanode under visible light illumination.

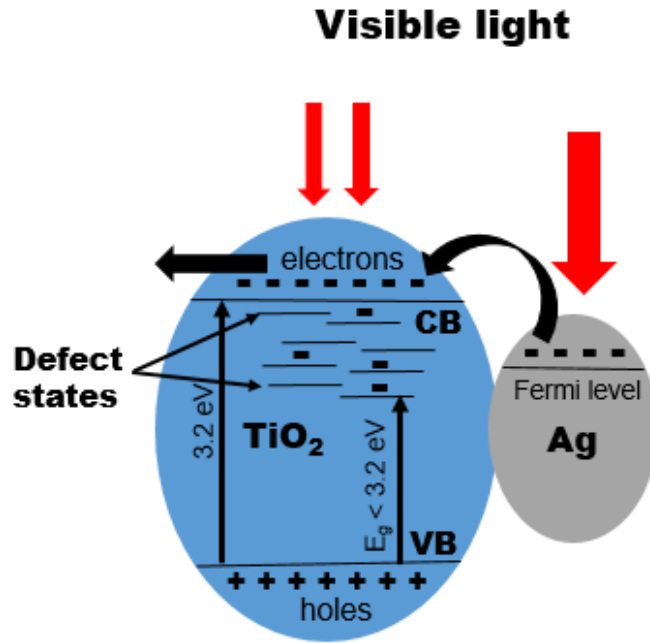


Figure 4.20: Schematic diagram for the charge separation and migration process of AgNPs/grassyTiNTs composite under visible light irradiation.

To evaluate the pure TiNTs and AgNPs/TiNTs at various pulse currents, a cell was constructed as previously described and then exposed to A.M. illumination (100 mW cm^{-2}). A rear-side-illuminated cell was used with a platinized counter electrode and iodine electrolyte. When light was irradiated into the cell, the dye was excited from the HOMO to the LUMO, and then the excited electrons were injected into the TiNTs' conduction band. For the AgNPs/TiNT-based DSSC, the excited electrons from the dye are thought to be first injected into the Ag NPs and subsequently transported to the conduction band of the TiNTs.

In addition to electrons from the dyes, electrons from the surface plasmons of Ag NPs would be transported to the conduction band of TiNTs, increasing the number of free electrons in the TiO₂ conduction band. Following electron transfer, the oxidized dye molecules are reduced by the electrolyte redox process. As the electrons are now transported to the TiNTs, they will go down to the back contact as quickly as possible to minimize the recombination inside the TiO₂ as well as with the dye and electrolyte.

The electron transport, however, is limited to the degree of scattering that can occur within the nanotubes as well as at the interface between the tube arrays and the titanium back contact. Nonetheless, utilizing a 1D nanotubular crystalline oxide may have eliminated most of the scattering, although the existence of secondary phases like rutile TiO₂, carbon-rich layers, or fluoride-rich layers at the interface between the TiNTs and the titanium sheet may impact the mobility of electrons. Electron transport from the titanium to the outside circuit must also be as scatter-free as possible to achieve high photocurrent generation. Thus, oxidation of the underlying titanium, which may occur during the annealing process of the TiNTs, may also impact the electron transport [59].

Ag NPs acts as electron collectors for the dyes. As a result, Ag NPs are thought to help in modifying the electronic properties at the metal-semiconductor interface. Now, because the Ag NPs have excess electrons on their surfaces, the position of the Fermi level of Ag NPs may have been moved closer to the conduction band of TiO₂ [120].

This means that electrons, whether from dyes or Ag NPs, can easily flow to TiNTs, resulting in an electron-rich photoanode. These electrons then proceed to the back contact, where photocurrent is created. Nonetheless, as the electrons move to the back contact, scattering may have happened, which explains why the photoconversion efficiency of the DSSC is still not as great as it is expected to be [121].

The results suggest that ordered and open 1D combined TiNTs-AgNPs array with uniform dispersion of Ag nanoparticles are useful for DSSC due to the combined effect of effective electron transport and enhanced plasmonic effect. In grassy TiNTs intraband gap defect states could act as trapping centres as shown in PL results which decreases the electron transfer and hence decreases the efficiencies of DSSCs as compared to open

TiNTs. However, it is worth noting that the presence of the optimum amount of Ag NPs on TiNTs promotes the development of significantly more efficient DSSCs which agrees with the PL results. In the PL spectra, the optimum amount of Ag NPs on open TiNTs at $15\text{mA}/\text{cm}^2$ showed lowest PL intensity, reduced recombination, and hence showed highest photoconversion efficiency in DSSC.

CHAPTER 5: CONCLUSIONS AND FUTURE RECOMMENDATION

5.1 Conclusion

TiNTs with two type morphologies were successfully produced using two-step anodization. One has an ordered morphology with open tube tops, while the other has nanoglass on the top surface as shown in SEM images. Both were loaded with AgNPs using the PCD method at varying pulse currents. By increasing pulse currents of 5 mA/cm^2 , average size of 10 nm approximately and average deposition of 10 weight % approximately of Ag NPs increases as shown in SEM and EDX results. It was discovered that order morphology promotes the homogeneous deposition of AgNPs on TiNTs. However, TiNTs covered with nanoglass do not have homogeneous deposition of Ag NPs as shown in SEM images. DSSC with a homogeneous distribution of Ag NPs on ordered open nanotubes at pulse current density of 15 mA/cm^2 exhibited the highest photoconversion efficiency (η) of 4.46%. However, DSSC with a non-homogeneous distribution of Ag NPs on grassy nanotubes at pulse current density of 10 mA/cm^2 exhibited the lowest photoconversion efficiency (η) of 2.85%.

These findings suggest that well aligned and nanoglass-free arrays, together with the optimum amount and uniform distribution of AgNPs, can greatly improve current conversion efficiencies in DSSCs. This is because grass reduces the plasmonic effect and effective electron transport from Ag NPs to the conduction band of TiO_2 due to the intra-band gap defect states as shown in PL results. Also, the optimal concentration of Ag NPs on TiNTs can improve photoconversion efficiency because if the Ag concentration is too low, the photo-generated charge carriers are not effectively separated due to insufficient contact between them. If the amount of Ag is too high, there is an increased possibility for the capture of holes by the large number of Ag nanoparticles, excessive coverage of Ag nanoparticles on surface of TiNTs increases reflection of incident light and may also decrease photoconversion efficiency in DSSCs. These investigations demonstrate that porous ordered 1D structures based on TiO_2 are critical for the great performance of DSSCs.

5.2 Future Recommendations

Various electrolytes, dyes, and photoanode materials have emerged because of the continuous development of dye-sensitized solar cells. A photoanode with superior electrical and optical qualities has yet to be considered for future research to make DSSCs economically viable. The PCD method for generating nanomaterials is widely recognized. There is a need to investigate the growth and shape of these materials in nanochannels made of TiO_2 . Other metal nanoparticles will be deposited on TiNTs for similar experiments. These investigations are intended to provide better control over the size, shape, and distribution of metal nanoparticles, resulting in improved properties and opening new opportunities for future DSSC applications.

REFERENCES

- [1] N. Asim *et al.*, "A review on the role of materials science in solar cells," *Renewable and sustainable energy reviews*, vol. 16, no. 8, pp. 5834-5847, 2012.
- [2] M. Vikas, S. Rao, and J. K. Seelam, "Tidal energy: a review," in *Proceedings of International Conference on Hydraulics, Water Resources and Coastal Engineering (Hydro2016)*, 2016.
- [3] M. Masood Ahmad, A. Kumar, and R. Ranjan, "Recent Developments of Tidal Energy as Renewable Energy: An Overview," *River and Coastal Engineering: Hydraulics, Water Resources and Coastal Engineering*, pp. 329-343, 2022.
- [4] E. F. WIND, "Wind Energy--Energy from Moving Air," *Int. J. Mar. Energy*, 2001.
- [5] W. Tong, *Fundamentals of wind energy*. WIT press Southampton, UK, 2010.
- [6] G. Caposciutti *et al.*, "Experimental investigation on biomass shrinking and swelling behaviour: particles pyrolysis and wood logs combustion," *Biomass and Bioenergy*, vol. 123, pp. 1-13, 2019.
- [7] E. Middelhoff, B. Madden, M. Li, F. Ximenes, M. Lenzen, and N. Florin, "Bioenergy siting for low-carbon electricity supply in Australia," *Biomass and Bioenergy*, vol. 163, p. 106496, 2022.
- [8] M. Guo, W. Song, and J. Buhain, "Bioenergy and biofuels: History, status, and perspective," *Renewable and sustainable energy reviews*, vol. 42, pp. 712-725, 2015.
- [9] D. C. Swain, "The Bureau of Reclamation and the New Deal, 1933-1940," *The Pacific Northwest Quarterly*, vol. 61, no. 3, pp. 137-146, 1970.
- [10] J. A. OMER, N. M. SARMAD, and E. SOLOMIN, "The Power Production Based on the Hydroelectric Turbine: A New approach," *Перспективы науки*, no. 11, pp. 18-25, 2018.

- [11] H. Saibi, S. Finsterle, R. Bertani, and J. Nishijima, "Geothermal energy," *Handbook of sustainable engineering*, pp. 1019-1042, 2013.
- [12] L. Kumar, M. S. Hossain, M. E. H. Assad, and M. U. Manoo, "Technological Advancements and Challenges of Geothermal Energy Systems: A Comprehensive Review," *Energies*, vol. 15, no. 23, p. 9058, 2022.
- [13] G. W. Crabtree and N. S. Lewis, "Solar energy conversion," *Physics today*, vol. 60, no. 3, pp. 37-42, 2007.
- [14] Y. Chu and P. Meisen, "Review and comparison of different solar energy technologies," *Global Energy Network Institute (GENI), San Diego, CA*, vol. 1, pp. 1-52, 2011.
- [15] A. Fahrenbruch, "RH Bube Fundamentals of solar cells Academic Press," *New York*, p. 119, 1983.
- [16] N. L. Panwar, S. C. Kaushik, and S. Kothari, "Role of renewable energy sources in environmental protection: A review," *Renewable and sustainable energy reviews*, vol. 15, no. 3, pp. 1513-1524, 2011.
- [17] T. Tsoutsos, N. Frantzeskaki, and V. Gekas, "Environmental impacts from the solar energy technologies," *Energy policy*, vol. 33, no. 3, pp. 289-296, 2005.
- [18] S. Sharma, K. K. Jain, and A. Sharma, "Solar cells: in research and applications—a review," *Materials Sciences and Applications*, vol. 6, no. 12, p. 1145, 2015.
- [19] K. Böer, "The physics and chemistry of solar cells," *Journal of Photochemistry*, vol. 10, no. 1, pp. 77-110, 1979.
- [20] M. Asadi and K. Pourhossein, "Neural network-based modelling of wind/solar farm siting: a case study of East-Azerbaijan," *International Journal of Sustainable Energy*, vol. 40, no. 7, pp. 616-637, 2021.

- [21] S. Yun, A. Hagfeldt, and T. Ma, "Pt-free counter electrode for dye-sensitized solar cells with high efficiency," *Advanced Materials*, vol. 26, no. 36, pp. 6210-6237, 2014.
- [22] J. Yan and B. R. Saunders, "Third-generation solar cells: a review and comparison of polymer: fullerene, hybrid polymer and perovskite solar cells," *Rsc Advances*, vol. 4, no. 82, pp. 43286-43314, 2014.
- [23] A. M. Bagher, "Introduction to organic solar cells," *Sustainable Energy*, vol. 2, no. 3, pp. 85-90, 2014.
- [24] I. Mauleón, "Photovoltaic investment roadmaps and sustainable development," *Journal of Cleaner Production*, vol. 167, pp. 1112-1121, 2017.
- [25] S. E. Manahan, *Environmental chemistry*. CRC press, 2022.
- [26] D. Cahen, G. Hodes, M. Grätzel, J. F. Guillemoles, and I. Riess, "Nature of photovoltaic action in dye-sensitized solar cells," *The Journal of Physical Chemistry B*, vol. 104, no. 9, pp. 2053-2059, 2000.
- [27] J. Gong, K. Sumathy, Q. Qiao, and Z. Zhou, "Review on dye-sensitized solar cells (DSSCs): Advanced techniques and research trends," *Renewable and Sustainable Energy Reviews*, vol. 68, pp. 234-246, 2017.
- [28] G. Boschloo and A. Hagfeldt, "Characteristics of the iodide/triiodide redox mediator in dye-sensitized solar cells," *Accounts of chemical research*, vol. 42, no. 11, pp. 1819-1826, 2009.
- [29] B. O'regan and M. Grätzel, "A low-cost, high-efficiency solar cell based on dye-sensitized colloidal TiO₂ films," *nature*, vol. 353, no. 6346, pp. 737-740, 1991.
- [30] P. Sommeling *et al.*, "Influence of a TiCl₄ post-treatment on nanocrystalline TiO₂ films in dye-sensitized solar cells," *The Journal of Physical Chemistry B*, vol. 110, no. 39, pp. 19191-19197, 2006.

- [31] J. Gong, J. Liang, and K. Sumathy, "Review on dye-sensitized solar cells (DSSCs): Fundamental concepts and novel materials," *Renewable and Sustainable Energy Reviews*, vol. 16, no. 8, pp. 5848-5860, 2012.
- [32] M. Grätzel, "Dye-sensitized solar cells," *Journal of photochemistry and photobiology C: Photochemistry Reviews*, vol. 4, no. 2, pp. 145-153, 2003.
- [33] Z.-S. Wang, H. Kawauchi, T. Kashima, and H. Arakawa, "Significant influence of TiO₂ photoelectrode morphology on the energy conversion efficiency of N719 dye-sensitized solar cell," *Coordination chemistry reviews*, vol. 248, no. 13-14, pp. 1381-1389, 2004.
- [34] M. Giannouli and F. Spiliopoulou, "Effects of the morphology of nanostructured ZnO films on the efficiency of dye-sensitized solar cells," *Renewable Energy*, vol. 41, pp. 115-122, 2012.
- [35] V. M. Ramakrishnan *et al.*, "Performance of TiO₂ nanoparticles synthesized by microwave and solvothermal methods as photoanode in dye-sensitized solar cells (DSSC)," *International Journal of Hydrogen Energy*, vol. 45, no. 51, pp. 27036-27046, 2020.
- [36] R. Dubey, K. V. Krishnamurthy, and S. Singh, "Experimental studies of TiO₂ nanoparticles synthesized by sol-gel and solvothermal routes for DSSCs application," *Results in Physics*, vol. 14, p. 102390, 2019.
- [37] H.-S. Chen, C. Su, C.-K. Lin, Y.-F. Hsieh, C.-K. Yang, and W.-R. Li, "Hydrothermal preparation of anatase TiO₂ nanoparticles for dye-sensitized solar cells," *Journal of Chemical Engineering of Japan*, vol. 42, no. Supplement., pp. s36-s42, 2009.
- [38] X. Hou, K. Aitola, and P. D. Lund, "TiO₂ nanotubes for dye-sensitized solar cells—A review," *Energy Science & Engineering*, vol. 9, no. 7, pp. 921-937, 2021.

- [39] H.-C. Lee, L.-F. Zhang, J.-L. Lin, Y.-L. Chin, and T.-P. Sun, "Development of anodic titania nanotubes for application in high sensitivity amperometric glucose and uric acid biosensors," *Sensors*, vol. 13, no. 10, pp. 14161-14174, 2013.
- [40] X. Liu *et al.*, "Large-diameter titanium dioxide nanotube arrays as a scattering layer for high-efficiency dye-sensitized solar cell," *Nanoscale Research Letters*, vol. 9, pp. 1-5, 2014.
- [41] S. Uchida, R. Chiba, M. Tomiha, N. Masaki, and M. Shirai, "Application of titania nanotubes to a dye-sensitized solar cell (e)," *ELECTROCHEMISTRY-TOKYO-*, vol. 70, no. 6, pp. 418-420, 2002.
- [42] J. M. Macák, H. Tsuchiya, A. Ghicov, and P. Schmuki, "Dye-sensitized anodic TiO₂ nanotubes," *Electrochemistry communications*, vol. 7, no. 11, pp. 1133-1137, 2005.
- [43] G. Senadeera, C. Thotawathage, and M. Dissanayake, "Efficiency enhancement in Dye Sensitized Solar Cells by light scattering in photoanode with TiO₂ nanotubes," in *Journal of Physics: Conference Series*, 2020, vol. 1552, no. 1, p. 012002: IOP Publishing.
- [44] N. S. Peighambaroust, S. K. Asl, R. Mohammadpour, and S. K. Asl, "Improved efficiency in front-side illuminated dye sensitized solar cells based on free-standing one-dimensional TiO₂ nanotube array electrodes," *Solar Energy*, vol. 184, pp. 115-126, 2019.
- [45] C.-N. Chen, Y.-W. Wang, Y.-R. Ho, C.-M. Chang, W.-C. Huang, and J.-J. Huang, "Liquid phase deposition/anodizing of TiO₂ nanotube working electrode for dye-sensitized solar cells," *Materials Science in Semiconductor Processing*, vol. 131, p. 105872, 2021.
- [46] T. Kasuga, M. Hiramatsu, A. Hoson, T. Sekino, and K. Niihara, "Formation of titanium oxide nanotube," *Langmuir*, vol. 14, no. 12, pp. 3160-3163, 1998.

- [47] S. Liu, L. Gan, L. Liu, W. Zhang, and H. Zeng, "Synthesis of single-crystalline TiO₂ nanotubes," *Chemistry of materials*, vol. 14, no. 3, pp. 1391-1397, 2002.
- [48] S. Sreekantan, K. A. Saharudin, Z. Lockman, and T. W. Tzu, "Fast-rate formation of TiO₂ nanotube arrays in an organic bath and their applications in photocatalysis," *Nanotechnology*, vol. 21, no. 36, p. 365603, 2010.
- [49] Y. Suzuki and S. Yoshikawa, "Synthesis and thermal analyses of TiO₂-derived nanotubes prepared by the hydrothermal method," *Journal of Materials Research*, vol. 19, pp. 982-985, 2004.
- [50] S. Chu, S. Inoue, K. Wada, S. Hishita, and K. Kurashima, "A new electrochemical lithography: Fabrication of self-organized titania nanostructures on glass by combined anodization," *Journal of the Electrochemical Society*, vol. 152, no. 3, p. B116, 2005.
- [51] T. R. Foong, Y. Shen, X. Hu, and A. Sellinger, "Template-directed liquid ALD growth of TiO₂ nanotube arrays: properties and potential in photovoltaic devices," *Advanced Functional Materials*, vol. 20, no. 9, pp. 1390-1396, 2010.
- [52] H. Shin, D. K. Jeong, J. Lee, M. M. Sung, and J. Kim, "Formation of TiO₂ and ZrO₂ nanotubes using atomic layer deposition with ultraprecise control of the wall thickness," *Advanced Materials*, vol. 16, no. 14, pp. 1197-1200, 2004.
- [53] D. Kowalski, D. Kim, and P. Schmuki, "TiO₂ nanotubes, nanochannels and mesosponge: Self-organized formation and applications," *Nano today*, vol. 8, no. 3, pp. 235-264, 2013.
- [54] S. Minagar, C. C. Berndt, J. Wang, E. Ivanova, and C. Wen, "A review of the application of anodization for the fabrication of nanotubes on metal implant surfaces," *Acta biomaterialia*, vol. 8, no. 8, pp. 2875-2888, 2012.
- [55] K. Chen *et al.*, "Effect of Ag nanoparticle size on the photoelectrochemical properties of Ag decorated TiO₂ nanotube arrays," *Journal of Alloys and Compounds*, vol. 554, pp. 72-79, 2013.

- [56] R. Asahi, T. Morikawa, T. Ohwaki, K. Aoki, and Y. Taga, "Visible-light photocatalysis in nitrogen-doped titanium oxides," *science*, vol. 293, no. 5528, pp. 269-271, 2001.
- [57] S. Chen, M. Paulose, C. Ruan, G. Mor, and O. Varghese, "Kouzoudis D and Grimes CA," *J. Photochem. Photobiol. A*, vol. 2006, p. 177, 2006.
- [58] L. Sun *et al.*, "Ultrasound aided photochemical synthesis of Ag loaded TiO₂ nanotube arrays to enhance photocatalytic activity," *Journal of Hazardous Materials*, vol. 171, no. 1-3, pp. 1045-1050, 2009.
- [59] N. Nyein, W. K. Tan, G. Kawamura, A. Matsuda, and Z. Lockman, "Anodic Ag/TiO₂ nanotube array formation in NaOH/fluoride/ethylene glycol electrolyte as a photoanode for dye-sensitized solar cells," *Nanotechnology*, vol. 27, no. 35, p. 355605, 2016.
- [60] S. Wang *et al.*, "Preferentially oriented Ag-TiO₂ nanotube array film: An efficient visible-light-driven photocatalyst," *Journal of Hazardous Materials*, vol. 399, p. 123016, 2020.
- [61] A. Sherly R, C. Padma, D. H. Raja, and D. J. Davidson, "Photodegradation of Methyl violet using Ag modified TiO₂ nanotubes by UV and UV/H₂O₂," *Chemical Physics Impact*, vol. 7, p. 100366, 2023.
- [62] M. Nycz, K. Arkusz, and D. G. Pijanowska, "Fabrication of electrochemical biosensor based on titanium dioxide nanotubes and silver nanoparticles for heat shock protein 70 detection," *Materials*, vol. 14, no. 13, p. 3767, 2021.
- [63] N. Farajpour, R. Deivanayagam, A. Phakatkar, S. Narayanan, R. Shahbazian-Yassar, and T. Shokuhfar, "A novel antimicrobial electrochemical glucose biosensor based on silver-Prussian blue-modified TiO₂ nanotube arrays," *Medical Devices & Sensors*, vol. 3, no. 2, p. e10061, 2020.

- [64] N. A. Jani *et al.*, "Photodeposition of Ag nanocrystals onto TiO₂ nanotube platform for enhanced water splitting and hydrogen gas production," *Journal of Nanomaterials*, vol. 2020, pp. 1-11, 2020.
- [65] N. A. Barakat, N. A. Erfan, A. A. Mohammed, and S. E. Mohamed, "Ag-decorated TiO₂ nanofibers as Arrhenius equation-incompatible and effective photocatalyst for water splitting under visible light irradiation," *Colloids and Surfaces A: Physicochemical and Engineering Aspects*, vol. 604, p. 125307, 2020.
- [66] J. Chen *et al.*, "Photo-functionalized TiO₂ nanotubes decorated with multifunctional Ag nanoparticles for enhanced vascular biocompatibility," *Bioactive Materials*, vol. 6, no. 1, pp. 45-54, 2021.
- [67] A. Perumal, S. Kannan, and R. Nallaiyan, "Silver nanoparticles incorporated polyaniline on TiO₂ nanotube arrays: A nanocomposite platform to enhance the biocompatibility and antibiofilm," *Surfaces and Interfaces*, vol. 22, p. 100892, 2021.
- [68] J.-C. Chou *et al.*, "AgNWs@ TiO₂ and AgNPs@ TiO₂ double-layer photoanode film improving light capture and application under low illumination," *Chemosensors*, vol. 9, no. 2, p. 36, 2021.
- [69] H. Ninsonti *et al.*, "Modified Sol-gel/Impregnation Synthesis of Titanium Dioxide Nanoparticles and Ag-loaded Titanium Dioxide Nanoparticles for Dye-Sensitized Solar Cells Application."
- [70] B. D. Choudhury, C. Lin, S. M. A. Z. Shawon, J. Soliz-Martinez, H. Huq, and M. J. Uddin, "A photoanode with hierarchical nanoforest TiO₂ structure and silver plasmonic nanoparticles for flexible dye sensitized solar cell," *Scientific reports*, vol. 11, no. 1, p. 7552, 2021.
- [71] B. Shougaijam and S. S. Singh, "Structural and optical analysis of Ag nanoparticle-assisted and vertically aligned TiO₂ nanowires for potential DSSCs application,"

Journal of Materials Science: Materials in Electronics, vol. 32, no. 14, pp. 19052-19061, 2021.

- [72] Y.-H. Nien *et al.*, "Study of how photoelectrodes modified by TiO₂/Ag nanofibers in various structures enhance the efficiency of dye-sensitized solar cells under low illumination," *Energies*, vol. 13, no. 9, p. 2248, 2020.
- [73] K. Bhojanaa, M. Ramesh, and A. Pandikumar, "Complementary properties of silver nanoparticles on the photovoltaic performance of titania nanospheres based photoanode in dye-sensitized solar cells," *Materials Research Bulletin*, vol. 122, p. 110672, 2020.
- [74] D. A. K. Ramadhani *et al.*, "Ag-doped TiO₂ as photoanode for high performance dye sensitized solar cells," *Materials Science for Energy Technologies*, 2024.
- [75] L. S. Pei, *Fabrication of Noble Metal Modified Titania Photoanode for Higher Efficiency Dye-Sensitized Solar Cells*. University of Malaya (Malaysia), 2015.
- [76] K. U. Isah, B. J. Jolayemi, U. Ahmadu, M. I. Kimpa, and N. Alu, "Plasmonic effect of silver nanoparticles intercalated into mesoporous betalain-sensitized-TiO₂ film electrodes on photovoltaic performance of dye-sensitized solar cells," *Materials for Renewable and Sustainable Energy*, vol. 5, pp. 1-9, 2016.
- [77] P. Chandrasekhar *et al.*, "Plasmonic silver nanowires for higher efficiency dye-sensitized solar cells," *Materials Today Energy*, vol. 5, pp. 237-242, 2017.
- [78] N. Irannejad, B. Rezaei, A. A. Ensafi, and N. Zandi-Atashbar, "Photovoltaic Performance Analysis of Dye-Sensitized Solar Cell Based on the Ag (4, 4'-Dicyanamidobiphenyl) Complex as a Light-Scattering Layer Agent and Linker Molecule on TiO₂ Photoanode," *IEEE Journal of Photovoltaics*, vol. 8, no. 5, pp. 1230-1236, 2018.
- [79] C. Liu *et al.*, "Silver nanoparticle modified TiO₂ nanotubes with enhanced the efficiency of dye-sensitized solar cells," *Microporous and Mesoporous Materials*, vol. 287, pp. 228-233, 2019.

- [80] W.-Y. Rho *et al.*, "Front-illuminated dye-sensitized solar cells with Ag nanoparticle-functionalized freestanding TiO₂ nanotube arrays," *Chemical Physics Letters*, vol. 614, pp. 78-81, 2014.
- [81] Y. Ren *et al.*, "Weak-light-driven Ag–TiO₂ photocatalyst and bactericide prepared by coprecipitation with effective Ag doping and deposition," *Optical Materials*, vol. 124, p. 111993, 2022.
- [82] N. U. Saqib, R. Adnan, and I. Shah, "Impact of silver ions doping and calcination on the physicochemical characteristics of TiO₂ nanoparticles with photocatalytic and regeneration potential," *Iranian Journal of Chemistry and Chemical Engineering*, vol. 40, no. 4, pp. 1012-1022, 2021.
- [83] M. A. Farkhondehfal *et al.*, "Syngas production by electrocatalytic reduction of CO₂ using Ag-decorated TiO₂ nanotubes," *International Journal of Hydrogen Energy*, vol. 45, no. 50, pp. 26458-26471, 2020.
- [84] J. Diaz-Real, P. Elsaesser, T. Holm, and W. Mérida, "Electrochemical reduction on nanostructured TiO₂ for enhanced photoelectrocatalytic oxidation," *Electrochimica Acta*, vol. 329, p. 135162, 2020.
- [85] X. Luan and Y. Wang, "Plasmon-enhanced performance of dye-sensitized solar cells based on electrodeposited Ag nanoparticles," *Journal of Materials Science & Technology*, vol. 30, no. 1, pp. 1-7, 2014.
- [86] T. Ghani, M. Mujahid, M. Mehmood, and G. Zhang, "Fabrication of self-branched TiO₂ nanotubes by anodization method, ordering and crystallinity," *Journal of Porous Materials*, vol. 26, pp. 193-203, 2019.
- [87] S. Ito *et al.*, "Fabrication of thin film dye sensitized solar cells with solar to electric power conversion efficiency over 10%," *Thin solid films*, vol. 516, no. 14, pp. 4613-4619, 2008.
- [88] C. S. Cojocaru *et al.*, "Conformal anodic oxidation of aluminum thin films," *Nano letters*, vol. 5, no. 4, pp. 675-680, 2005.

- [89] P. Sheasby, R. Pinner, and S. Wernick, "The surface treatment and finishing of aluminium and its alloys, ASM International," *Wu, L., Wen, C., Zhang, G., Liu, J., Ma, K.(2017) Influence of anodizing time on morphology, structure and tribological properties of composite anodic films on titanium alloy. Vacuum*, vol. 140, pp. 176-184, 2001.
- [90] C. Larson and J. Farr*, "Current research and potential applications for pulsed current electrodeposition—a review," *Transactions of the IMF*, vol. 90, no. 1, pp. 20-29, 2012.
- [91] A. Lelevic and F. C. Walsh, "Electrodeposition of NiP composite coatings: A review," *Surface and Coatings Technology*, vol. 378, p. 124803, 2019.
- [92] M. Chandrasekar and M. Pushpavanam, "Pulse and pulse reverse plating—Conceptual, advantages and applications," *Electrochimica Acta*, vol. 53, no. 8, pp. 3313-3322, 2008.
- [93] A. Roy, A. Ghosh, S. Bhandari, P. Selvaraj, S. Sundaram, and T. K. Mallick, "Color comfort evaluation of dye-sensitized solar cell (DSSC) based building-integrated photovoltaic (BIPV) glazing after 2 years of ambient exposure," *The Journal of Physical Chemistry C*, vol. 123, no. 39, pp. 23834-23837, 2019.
- [94] A. Sacco *et al.*, "Microfluidic housing system: a useful tool for the analysis of dye-sensitized solar cell components," *Applied Physics A*, vol. 109, pp. 377-383, 2012.
- [95] A. Ali, Y. W. Chiang, and R. M. Santos, "X-ray diffraction techniques for mineral characterization: A review for engineers of the fundamentals, applications, and research directions," *Minerals*, vol. 12, no. 2, p. 205, 2022.
- [96] T. Fawcett *et al.*, "A practical guide to pharmaceutical analyses using X-ray powder diffraction," *Powder Diffraction*, vol. 34, no. 2, pp. 164-183, 2019.
- [97] G. Artioli, "X-Ray Diffraction," in *Encyclopedia of Geoarchaeology*: Springer, 2022, pp. 1-7.

- [98] G. Gentile *et al.*, "A brief review of scanning electron microscopy with energy-dispersive X-ray use in forensic medicine," *The American Journal of Forensic Medicine and Pathology*, vol. 41, no. 4, pp. 280-286, 2020.
- [99] N. Ural, "The significance of scanning electron microscopy (SEM) analysis on the microstructure of improved clay: An overview," *Open Geosciences*, vol. 13, no. 1, pp. 197-218, 2021.
- [100] D. Moro, G. Ulian, and G. Valdre, "SEM-EDS nanoanalysis of mineral composite materials: A Monte Carlo approach," *Composite Structures*, vol. 259, p. 113227, 2021.
- [101] P. Zimmermann *et al.*, "Modern X-ray spectroscopy: XAS and XES in the laboratory," *Coordination Chemistry Reviews*, vol. 423, p. 213466, 2020.
- [102] E. Smith and G. Dent, *Modern Raman spectroscopy: a practical approach*. John Wiley & Sons, 2019.
- [103] J. Moon, M. Li, A. J. Ramirez-Cuesta, and Z. Wu, "Raman spectroscopy," in *Springer Handbook of Advanced Catalyst Characterization*: Springer, 2023, pp. 75-110.
- [104] D. Kourouski, A. Dazzi, R. Zenobi, and A. Centrone, "Infrared and Raman chemical imaging and spectroscopy at the nanoscale," *Chemical Society Reviews*, vol. 49, no. 11, pp. 3315-3347, 2020.
- [105] T. Kirchartz, J. A. Márquez, M. Stolterfoht, and T. Unold, "Photoluminescence-based characterization of halide perovskites for photovoltaics," *Advanced energy materials*, vol. 10, no. 26, p. 1904134, 2020.
- [106] M. A. Reshchikov, "Measurement and analysis of photoluminescence in GaN," *Journal of Applied Physics*, vol. 129, no. 12, 2021.

- [107] M. Abdi-Jalebi, M. I. Dar, A. Sadhanala, E. M. Johansson, and M. Pazoki, "Optical absorption and photoluminescence spectroscopy," in *Characterization Techniques for Perovskite Solar Cell Materials*: Elsevier, 2020, pp. 49-79.
- [108] H. Tian, G. Boschloo, and A. Hagfeldt, *Molecular devices for solar energy conversion and storage*. Springer, 2018.
- [109] Z. Zhang, M. F. Hossain, and T. Takahashi, "Photoelectrochemical water splitting on highly smooth and ordered TiO₂ nanotube arrays for hydrogen generation," *International journal of hydrogen energy*, vol. 35, no. 16, pp. 8528-8535, 2010.
- [110] A. Mazzarolo, K. Lee, A. Vincenzo, and P. Schmuki, "Anodic TiO₂ nanotubes: Influence of top morphology on their photocatalytic performance," *Electrochemistry communications*, vol. 22, pp. 162-165, 2012.
- [111] F. Ahmed *et al.*, "Fabrication of TiO₂-nanotube-array-based supercapacitors," *Micromachines*, vol. 10, no. 11, p. 742, 2019.
- [112] L. Sang, H. Ge, and B. Sun, "Probing plasmonic Ag nanoparticles on TiO₂ nanotube arrays electrode for efficient solar water splitting," *International Journal of Hydrogen Energy*, vol. 44, no. 30, pp. 15787-15794, 2019.
- [113] C. Su, L. Liu, M. Zhang, Y. Zhang, and C. Shao, "Fabrication of Ag/TiO₂ nanoheterostructures with visible light photocatalytic function via a solvothermal approach," *CrystEngComm*, vol. 14, no. 11, pp. 3989-3999, 2012.
- [114] X. Fan *et al.*, "High-efficiency photoelectrocatalytic hydrogen generation enabled by Ag deposited and Ce doped TiO₂ nanotube arrays," *Ceramics International*, vol. 41, no. 3, pp. 5107-5116, 2015.
- [115] M. Ubaidullah *et al.*, "Preparation of composite-layered structure of TiO₂ nanoparticles/TiO₂ nanotubes and its role in dye sensitized solar cell," *Journal of Porous Materials*, vol. 28, pp. 555-566, 2021.

- [116] A. Hajjaji, M. Elabidi, K. Trabelsi, A. Assadi, B. Bessais, and S. Rtimi, "Bacterial adhesion and inactivation on Ag decorated TiO₂-nanotubes under visible light: Effect of the nanotubes geometry on the photocatalytic activity," *Colloids and Surfaces B: Biointerfaces*, vol. 170, pp. 92-98, 2018.
- [117] M. Gaidi *et al.*, "Optimizing the photochemical conversion of UV–vis light of silver-nanoparticles decorated TiO₂ nanotubes based photoanodes," *Nanotechnology*, vol. 29, no. 1, p. 015703, 2017.
- [118] N. Pugazhenthiran, S. Murugesan, and S. Anandan, "High surface area Ag-TiO₂ nanotubes for solar/visible-light photocatalytic degradation of ceftiofur sodium," *Journal of hazardous materials*, vol. 263, pp. 541-549, 2013.
- [119] L. Yu, X. Yang, Y. Ye, X. Peng, and D. Wang, "Silver nanoparticles decorated anatase TiO₂ nanotubes for removal of pentachlorophenol from water," *Journal of colloid and interface science*, vol. 453, pp. 100-106, 2015.
- [120] M. Ni, "KH., Leung DYC. and Sumathy K.,", "A review and recent developments in photocatalytic water-splitting using for hydrogen production, pp. 401-425, 2007.
- [121] Y. F. Wang, J. H. Zeng, and Y. Li, "Silver/titania nanocable as fast electron transport channel for dye-sensitized solar cells," *Electrochimica Acta*, vol. 87, pp. 256-260, 2013.